



Review

A Review of Fluid Energy Converters Based on Triboelectric Nanogenerators: Performance Analysis from Energy Conversion

Qianying Li and Yi Xi *

Chongqing Key Laboratory of Soft Condensed Matter Physics and Smart Materials, Department of Applied Physics, Chongqing University, Chongqing 400044, China; liqy@cqu.edu.cn

* Correspondence: yxi6@cqu.edu.cn

Abstract: In recent years, the development of the Internet of Things has challenged traditional energy supply methods. Suddenly rising maintenance costs and serious environmental pollution have led to great concern over energy supply methods such as wired transmission and batteries. Fluid energy is a kind of clean energy widely existing in nature, which can effectively reduce costs and environmental pollution. In the field of collecting fluid energy, fluid energy converters based on triboelectric nanogenerators (FEC-TENGs) have always been a research hotspot. This paper reviews the latest research progress of FEC-TENGs. Firstly, the basic working principle and working mode of FEC-TENGs are introduced. Then, the theoretical process and application examples of converting fluid energy into electrical energy or electrical signals are analyzed in detail. According to the calculation process of energy conversion efficiency and the performance evaluation parameters, the structural design, performance output, and application fields of FEC-TENGs are summarized. Finally, this paper points out the challenges and shortcomings of the current FEC-TENGs and provides our views on the future development of this field.

Keywords: fluid energy; triboelectric nanogenerator; energy conversion; water energy; wind energy



Citation: Li, Q.; Xi, Y. A Review of Fluid Energy Converters Based on Triboelectric Nanogenerators: Performance Analysis from Energy Conversion. *Nanoenergy Adv.* **2023**, *3*, 282–314. <https://doi.org/10.3390/nanoenergyadv3040016>

Academic Editors: Ya Yang and Sang Min Lee

Received: 21 July 2023

Revised: 1 September 2023

Accepted: 27 September 2023

Published: 8 October 2023



Copyright: © 2023 by the authors. Licensee MDPI, Basel, Switzerland. This article is an open access article distributed under the terms and conditions of the Creative Commons Attribution (CC BY) license (<https://creativecommons.org/licenses/by/4.0/>).

1. Introduction

As one of the most important and abundant energy sources in nature, fluid energy is a kind of renewable energy widely existing in gas and liquid [1,2]. As one of the important sources of clean energy, fluid energy is widely distributed in nature, including wind energy, airflow energy, water energy, wave energy, and so on [3–5]. Wind energy and airflow energy are the energy generated by the flow of air, which is generally used to drive the power device of the generator [6,7]. Water energy and ocean energy refer to the energy generated by the flow of water, which can be captured and converted into electrical energy [5,8,9]. Different from other energy dependence on season, day and night, weather, and temperature, fluid energy is distributed in every corner of our lives, showing strong competitiveness [3]. They all can be captured and converted into electrical energy. However, fluid energy, especially wind and water energy, not only has a small frequency of motion (<4 Hz), but also the direction of motion of wind and water is irregular, which undoubtedly increases the difficulty in designing energy harvesters [10]. Most energy harvesters based on electromagnetic generators (EMGs) suffer from low matching frequency, large volume, high replacement cost, and susceptibility to corrosion when collecting fluid energy [11]. For piezoelectric nanogenerators (PENGs), the piezoelectric material is sandwiched between two electrodes [12]. If the device is subjected to a compressive or tensile force, a potential difference is created between the electrodes, which drives the flow of electrons in the external circuit, generating an electric current [13]. Although PENGs can efficiently convert mechanical energy into electrical energy, strict material selection rules and the single working mode make them slightly inferior in harvesting fluid energy [13–15].

Thermoelectric generators (TEGs) convert thermal energy into electrical energy through the Seebeck effect or the Soret effect [12]. However, the small output of TEGs and the requirement of temperature difference limit its development. Therefore, the development of a low-frequency fluid energy collector with small size, low cost, easy replacement, low environmental requirements, rich material selection, and various working modes can realize the development and utilization of these fluid energy sources, which is very important for achieving sustainable energy development and reducing carbon emissions.

Founded on the principles of triboelectrification and electrostatic induction, the triboelectric nanogenerators (TENGs) were first invented by Wang's team in 2012 [16,17]. Since its invention, TENGs have developed rapidly and attracted more than 4000 scientists to study them [18,19]. TENG not only has a variety of structural designs and low production costs, but it also has a wealth of material choices and a variety of working modes, which is very suitable for the collection of fluid energy [13,14]. According to the output characteristics of TENGs, they can be divided into alternating-current TENGs (AC-TENGs) and direct-current TENGs (DC-TENGs) [20–25]. Whether it is AC-TENGs or DC-TENGs, their material selection is very extensive, involving ordinary clothing fiber expansion, most organic synthesis, metallic glass, and other materials [26–29]. A wide range of material choices combined with a variety of structural designs make TENGs outstanding in the four major areas of micro/nano-energy, self-powered sensors, blue energy, and high-voltage sources [17,30–33]. In particular, as a low-frequency environmental mechanical energy harvester, TENGs are handy in collecting fluid energy well [3,34]. However, FEC-TENGs also face a series of problems. Due to the lack of necessary theoretical support, a large number of excellent devices have a single way to improve their output. Due to their low energy conversion efficiency, FEC-TENGs have struggled to achieve industrialization. Related research has developed from the most common energy collection to related research based on fluid mechanics, and even to the specific analysis of the energy transfer process [35–37]. Although FEC-TENGs have developed rapidly and received a lot of reports, there is still a lack of comprehensive comparison and summary on the working mode of the device, the energy transfer process and transfer efficiency, the performance comparison of the system, and the main application fields.

Here, aiming at improving the overall performance of FEC-TENGs, and promoting the future commercialization of FEC-TENGs, this review is divided into four parts: the basic working modes of FEC-TENGs, the theoretical analysis and application examples of the energy transfer process based on FEC-TENGs, the structural design and performance evaluation of FEC-TENGs, and the application summary of FEC-TENGs. Figure 1 shows the core concept of this review. Finally, this review points out the shortcomings, challenges, and future research priorities in the field of FEC-TENGs, aiming to guide the development of the next-generation FEC-TENGs. Furthermore, it points the way to effectively improve the energy conversion efficiency of FEC-TENGs and provides a useful reference for researchers focusing on fluid energy collection.



Figure 1. Performance parameters and energy conversion of FEC-TENGs. Reprinted with permission from Ref. [7]. Copyright 2017, Wiley. Reprinted with permission from Ref. [17]. Copyright 2020, Wiley. Reprinted with permission from Ref. [36]. Copyright 2022, Elsevier. Reprinted with permission from Ref. [37]. Copyright 2021, Elsevier. Reprinted with permission from Ref. [38]. Copyright 2020, Elsevier. Reprinted with permission from Ref. [39]. Copyright 2021, Wiley. Reprinted with permission from Ref. [40]. Copyright 2019, Elsevier. Reprinted with permission from Ref. [41]. Copyright 2022, American Chemical Society. Reprinted with permission from Ref. [42]. Copyright 2021, Springer Nature. Reprinted with permission from Ref. [43]. Copyright 2019, Wiley. Reprinted with permission from Ref. [44]. Copyright 2021, Wiley. Reprinted with permission from Ref. [45]. Copyright 2022, Elsevier.

2. Basic Working Mode of FEC-TENGs

With the development of TENGs, fluid energy converters based on TENGs mainly include water energy collectors and wind energy collectors. They were both invented based on the coupling of contact electrification and electrostatic induction effect and have played a great role in energy conservation and emission reduction. In this section, we first introduce the basic theory of TENGs, then discuss the four basic working modes of TENGs and the applicable working modes of FEC-TENGs. Finally, we propose the more inclined working modes of FEC-TENGs and explain the reasons.

2.1. Basic Theory of TENGs

As the theoretical origin of TENGs, Maxwell’s displacement current is defined as follows:

$$J_D = \frac{\partial D}{\partial t} = \epsilon_0 \frac{\partial E}{\partial t} + \frac{\partial P}{\partial t}, \quad (1)$$

where D , E , and P represent the displacement field, electric field, and polarization field density, respectively. ϵ_0 is the vacuum permittivity. The first term of displacement current unifies electric and magnetic fields, predicting the existence of electromagnetic waves [46,47]. In a generally isotropic medium, the first and second terms are combined, so the direct relationship between displacement current and energy is difficult to reveal. However, when there are surface polarized charges in the medium, the displacement current has a

contribution to the polarization density caused by the surface electrostatic charges- P_s , also known as the Wang term [16,17,48].

$$J_D = \frac{\partial D}{\partial t} = \epsilon \frac{\partial E}{\partial t} + \frac{\partial P_s}{\partial t}, \tag{2}$$

where ϵ is the dielectric constant. P_s is the current caused by the polarization field generated by the electrostatic charge on the surface of the medium, which is the fundamental theoretical basis of TENGs [5,49].

2.2. Basic Working Modes of FEC-TENGs

To cope with the complex energy harvesting environment and better harvest the dispersed mechanical energy in the environment, four basic working modes have been proposed for TENG according to the polarization change direction and electrode configuration, including vertical contact/separation (CS) mode, lateral-sliding (LS) mode, single-electrode (SE) mode, and freestanding triboelectric-layer (FT) mode [26,50].

Taking the working mode of contact/separation as an example, the working principle of TENGs is explained in detail below. As shown in Figure 2a, the basic contact/separation mode is formed by stacking two different tribo-dielectric films face-to-face, while their backsides are plated with metal electrodes. Since the electronegativity of the two dielectric layers is different in the triboelectric series [29,51], the physical contact between them will cause the triboelectric film to be charged with opposite signs (Figure 2a(i)). When the two surfaces are separated by mechanical force, an air gap is formed between the two tribo-dielectric films. In this process, the external force overcomes the electrostatic attraction and the elastic energy of the material itself to do work, providing the input energy of TENGs, which in turn generates a potential difference. When the back electrodes are connected by a load, free-moving electrons flow from one electrode to the other to balance the potential difference, forming a current in the external load (Figure 2a(ii,iii)). When the external mechanical force continues to act on the TENG, the potential difference formed by the triboelectric charges disappears and the electrons flow back to the original electrode (Figure 2a(iv)). Repeating the above four steps, TENG continuously forms a pulsed alternating current (AC) output in the external circuit [52]. The other three working modes are shown in Figure 2b–d. Since much literature has already introduced them in detail, this article will not repeat them [46,53].

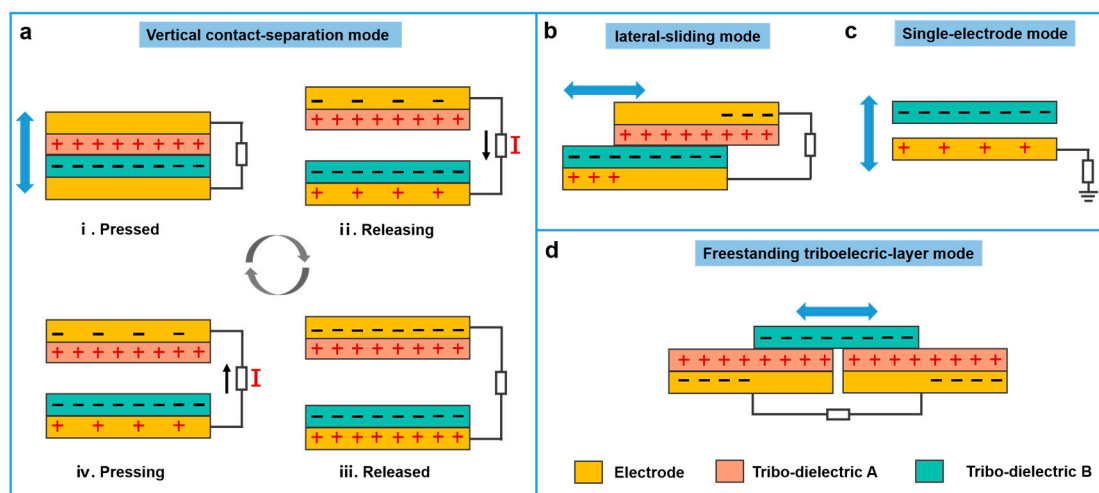


Figure 2. Four basic working modes of TENGs: (a) Vertical CS mode. (b) LS mode. (c) SE mode. (d) FT mode.

Interestingly, some hybrid generators based on TENG and other generators combine multiple working modes to efficiently collect fluid energy [54,55]. In general, TENGs

are mostly combined with PENGs and EMGs, which can effectively improve the energy conversion efficiency of hybrid generators [54,56]. For example, the combination of TENGs and PENGs is one of the best ways to optimize the performance of a single device [54]. Mariello et al. designed a biocompatible hybrid nanogenerator (HNG) for collecting hydro-energy [57]. This HNG is assembled based on thin-film piezoelectric ceramics and soft polymer materials and can be used to collect different forms of water energy. In addition, the combination of TENGs and EMGs further broadens the frequency range of the device for collecting fluid energy [56]. TENGs perform well in collecting low-frequency fluid energy [54]. EMGs play an important role in collecting high-frequency fluid energy [56]. Based on TENG and EMG, Ren et al. developed a hybrid wave energy harvesting nanogenerator (HW-NG) as a power source for remote wireless transmission by designing a pendulum structure [58]. The HW-NG integrates the complementary advantages of TENG and EMG so that it can obtain satisfactory output in a wide operating frequency range. Furthermore, the combination of TENGs with solar cells and thermoelectric generators further enriches the working mode of the fluid energy collector [59,60]. In the follow-up discussion of this review, we have covered the above hybrid generators, while focusing on comparing the performance of TENGs.

It has to be mentioned that the working principle of some FEC-TENGs that collect raindrop energy is different from the above working principle. It is well known that raindrop energy generally contains two kinds of energy: the gravitational potential energy of raindrops and the electrostatic energy generated by contact friction with air or dielectric materials [54]. The gravitational potential energy of the raindrops can cause the raindrops to hit the TENGs, driving the working unit of the TENGs to operate periodically, thereby collecting energy. The first waterproof, fabric-based multifunctional TENG (WPF-MTENG) was designed by Lai et al., and its working mode is the CS mode [61]. The soft and elastic properties of the fabric enable it to convert slight shocks such as raindrops into contact separation between two internally moving fabrics and generate electrical output [61]. However, the impact force of raindrops is limited, and similar devices face problems such as low output and difficulty in the direct use of energy [54]. Therefore, a droplet-based generator (DEG) consisting of a polytetrafluoroethylene film on an indium tin oxide substrate and an aluminum electrode was developed [62]. The impact water droplets connect the originally disconnected components into a closed-loop electronic system, transforming the interface effect into a volume effect, thereby increasing the instantaneous power density by several orders of magnitude [62]. Since then, several efforts have been made to optimize and integrate DEG [63]. For example, the reasonable electrode design of DEG is used to avoid the cancellation of electrical signals between adjacent raindrops [64]. A simple open-structure droplet generator is obtained by using the self-capacitance effect of the upper electrode [65]. Moreover, based on the concept of full current, a unique bionic DC-TENG is proposed. By using water charge shuttle (WCS) architecture, it can directly convert the fluid kinetic energy into high-voltage direct current energy through solid-liquid contact electrification, and it performs well in collecting raindrop energy [66]. For FEC-TENGs that collect the electrostatic energy of raindrops, raindrops are mainly used as an electropositive friction material. Their working principle is similar to that of TENG based on the FT mode [67].

2.3. Material Selection of FEC-TENGs

Considering the special working environment of FEC-TENGs, there are certain requirements for the production of triboelectric materials for FEC-TENGs. First, FEC-TENGs working outdoors should be able to adapt to humid and water-permeable environments. At the same time, the choice of water-resistant and moisture-resistant materials is also a favorable measure [55]. Therefore, some commonly used hydrophobic materials are often used in FEC-TENGs, such as Polytetrafluoroethylene (PTFE), Polydimethylsiloxane (PDMS), Fluorinated ethylene propylene (FEP), Polyvinylidene fluoride (PVDF), and other materials [55]. In addition, FEC-TENGs with hydrophobic materials can operate effectively

for a long time [68]. On the one hand, for unpackaged devices, water is in direct contact with the interface of triboelectric materials. Water is generally used as an electropositive material, and hydrophobic materials are used as electronegative materials. Hydrophobic materials are conducive to accelerating the flow, diffusion, and complete separation of water, which is of great significance for enhancing the electrostatic induction effect, reducing electrostatic shielding, and achieving higher triboelectric output [69]. On the other hand, hydrophobic materials also have the characteristics of self-cleaning, anti-icing, and anti-sticking, which can effectively reduce the signal attenuation caused by direct contact with water [70,71].

Moreover, to achieve high output performance and durability, the selection of durable triboelectric materials is also crucial for FEC-TENGs. As mentioned above, some common electronegative materials for FEC-TENGs include PTFE, PDMS, FEP, etc. [3]. At the same time, some common positive materials include copper electrodes, aluminum electrodes, nylon, and other materials [5]. In recent years, some soft furs have also been used as electropositive materials to reduce wear between materials [31]. In addition to reducing the wear between materials, the study of wear-resistant and high-performance triboelectric materials can also effectively improve the performance of FEC-TENGs [72,73]. For example, as a promising triboelectric material, butyl melamine formaldehyde (BMF) has excellent mechanical durability and triboelectric positivity [72]. The wear rate of BMF is lower than that of PTFE in the wear test with copper as the auxiliary friction material, and it remains stable in the test of 27,000 cycles [72]. Moreover, N-dihydroxyurea (DMU), diazolyurea (DU), and imidazolyurea (IU) can also be used as highly tribopositive materials [73]. Since nitrogen-based materials are rich in nitrogen and oxygen, they provide high surface potential and triboelectric output. Among them, IU showed better performance than nylon, DMU, and DU [73].

Interestingly, recently, the use of biodegradable materials to make FEC-TENGs has become an environmentally friendly, sustainable concept [74]. Feng et al. made degradable FEC-TENGs using fresh tobacco leaves as friction materials to collect wind energy [75]. Choi et al. deposited metal on the back of the surface of natural lotus leaves to produce natural lotus leaf TENG (LL-TENG) [76]. Through water droplets falling on the surface of LL-TENG, electricity is generated spontaneously [76]. However, the degradability of the material will lead to the gradual attenuation of device performance and the sudden failure of the device. We will propose solutions for such FEC-TENGs.

In summary, the selection of high-performance triboelectric materials is always important for researchers studying FEC-TENGs. Among these materials, if a material has excellent mechanical stability, excellent waterproof ability or hydrophobic ability, and is environmentally friendly, it is considered the best.

2.4. Summary of the Working Modes of the FEC-TENGs

For the collection of fluid energy, water energy collectors and wind energy collectors focus on different working modes. As for water energy collectors, they need to convert irregular and low-frequency water wave motion into a regular energy output. Therefore, the vertical CS mode, with which the above effects can be easily achieved, has been the focus of research. In Figure 3a, Ren et al. proposed a hybrid wave energy harvesting nanogenerator (HW-NG) as a power source for remote wireless transmission [58]. The TENG unit is based on the working mode of contact separation and is designed as a spring-assisted multi-layer structure. The working cycle period is shown in the illustrations i-iv in Figure 3a. The HW-NG utilized a simple pendulum structure to effectively combine contact-separated TENGs and electromagnetic generators (EMGs), which can efficiently collect wave energy [58]. Moreover, in Figure 3b, Zhang et al. exploited the CS mode and resonance effects to harvest omnidirectional and frequency-varying water wave energy by ingeniously combining pendulums, rollers, and flexible rings [37]. Interestingly, in Figure 3c, Deng et al. introduced the gas pocket exchange structure of paired TENGs and a rigid/flexible coupling deformation mechanism, and the device achieved efficient

operation in a contact-separated mode even in deep water [77]. Moreover, thanks to the simple design of the CS mode and its high adaptability to a large number of structures, water energy collectors based on the CS mode have been widely adopted [35,36,78].

Different from the CS mode, the FT mode has higher requirements on the structure design and size, but it is more efficient and continuous when collecting energy [31,79]. Therefore, the water energy harvester based on the FT mode is also the focus of research at present [47]. As shown in Figure 3d, Bai et al. demonstrated a high-performance tandem-disk TENG (TD-TENG) for self-powered water quality monitoring by designing an FS mode-based radial grating structure [40]. In Figure 3e, a fully symmetrical TENG (EC-TENG) with an elliptical cylindrical swing structure was designed by Tan et al. to collect all-weather blue energy [80]. The internal TENG of EC-TENG adopts an independent structure with steel bars as rolling elements. Under slight stimulation, the steel rod exhibits flexible rolling activity, so that the internal TENG can effectively capture water wave energy in a calm ocean [80]. Combined with the hierarchical transmission unit, the working mode of the hierarchical energy harvesting TENG (GEH-TENG) proposed by Xu et al. is a typical FS mode [81]. In Figure 3f, when the swing of GEH-TENG begins to be driven by waves, the soft FEP film slides on the stator composed of copper foil as a slider of the FT mode. The blade-like design makes the contact between the friction layers tight and difficult to wear. Recently, as shown in Figure 3g, by introducing soft hairs in combination with the FT mode of operation, water energy harvesters have both increased output and extended device durability [41,44,82]. From the above summary of the working mode of the water energy collector, it can be seen that the researchers are more inclined to design structures with a high output response under a low-frequency drive to collect low-frequency water wave energy. Therefore, the TENG that collects water wave energy mostly adopts the CS working mode. Since the traditional TENG based on the FT working mode requires a larger driving force, some ingenious structural designs are used to reduce the resistance encountered by the triboelectric layers during the movement of the TENG, such as using sticks [80], leaves [83], and soft animal fur, as the triboelectric layers [31].

Similar to water energy harvesters, most studies on TENG-based wind energy harvesters focus on CS mode and FT mode. Interestingly, in Figure 4a, Yuan et al. developed a wake-galloping-driven TENG (WG-TENG) based on the wake-galloping effect. The unique dynamic characteristics of the effect enable the device to efficiently collect breeze wind energy in a slight CS mode [45]. In addition, this WG-TENG is easy to manufacture and can be combined with packaging boxes, water bottles, and books to collect wind energy. In Figure 4b, the most typical representative of wind energy harvesters using CS mode is the flutter-effect-based TENG (FE-TENG) designed by Hu et al. [6]. Based on the flutter effect, when the natural wind passes through the polyethylene terephthalate (PET) tape, the flutter of the PET tape causes the oscillation of the silicon sphere suspended under the tape. The strong impact of the ball on the FE-TENG unit makes it contact and separate. Interestingly, the fully symmetrical design of FE-TENG enables it to collect breeze energy in any direction. Another new type of TENG based on the flow-induced vibration (FIV) effect and CS working mode also has excellent performance in collecting breeze energy, which we will discuss systematically later [38]. Similarly, based on the FIV effect, a TENG, which can capture multi-directional wind energy, has collected $1.8\text{--}4.3\text{ m s}^{-1}$ of breeze energy [39]. Based on the theory of fluid mechanics, the wind impact model of the TENG is established. The force analysis of the model and the dynamic model of mechanical energy and electrical energy conversion are analyzed carefully. In addition, Zhu et al. designed a double-blade structured triboelectric–electromagnetic hybrid generator (DB-TEHG) [84]. In the TENG part, DB-TEHG adopts the CS working mode. At the same time, the author used fluid mechanics to simulate and optimize the blade parameters, which improved the aerodynamic performance of DB-TENG. Secondly, because the CS mode can effectively reduce the wear and tear of the device, some wind energy collectors convert the energy obtained by the rotation mode into the energy obtained by the CS mode through structural design [85–88]. In Figure 4c, Gao et al. successfully combined the CS mode and rotational

structure through the design of turbine disks, which effectively improved the durability of the device [85]. In Figure 4d, a self-powered NO_x absorption and degradation system realized the harvesting of rotational energy in CS mode through the combination of piston motion and radial engine-shaped TENG [89].

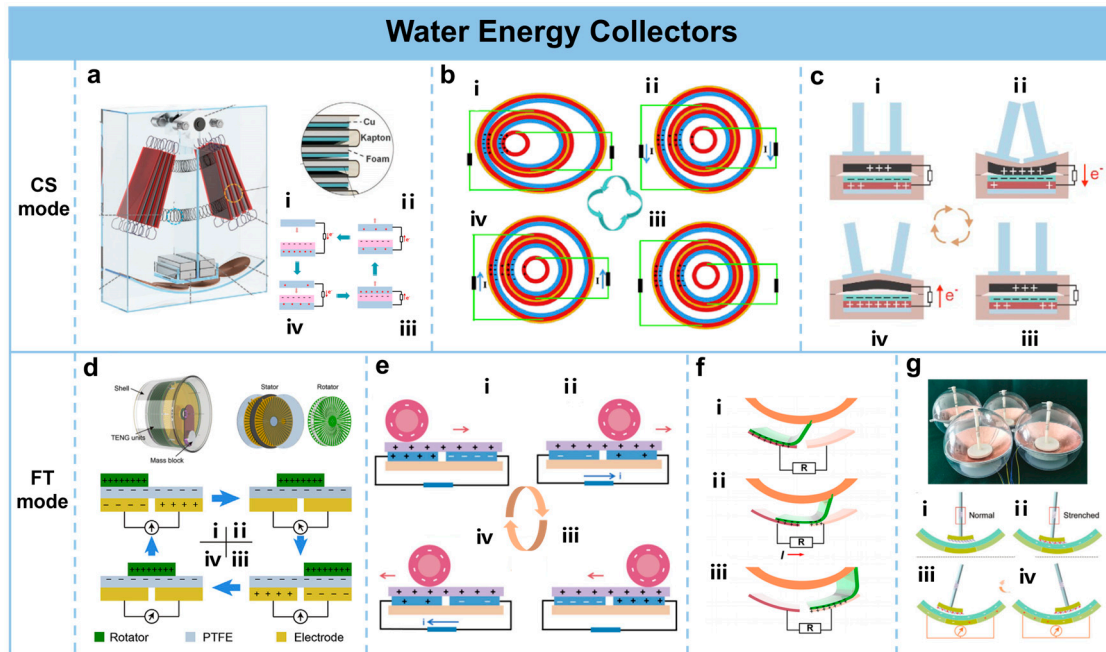


Figure 3. Systematic summary of TENG for collecting water energy based on CS mode and FT mode working mode: (a–c) Examples of TENG collecting water energy using CS working mode. (a) The CS-mode TENG designed as a spring-assisted multilayer structure to form a hybrid wave energy harvesting nanogenerator. Illustration i–iv is the working schematic diagram. Reprinted with permission from Ref. [58]. Copyright 2021, Wiley. (b) An active resonant TENG (AR-TENG) system composed of a single pendulum, a pendulum and flexible ring, which will produce two contact separation processes in one wave. Illustration i–iv is the working schematic diagram. Reprinted with permission from Ref. [37]. Copyright 2021, Elsevier. (c) High-performance paired TENG (P-TENG) working in deep water. Driven by the vibration of the pillar, the upper layer of the P-TENG is deformed and the CS movement is realized. Illustration i–iv is the working schematic diagram. Reprinted with permission from Ref. [77]. Copyright 2022, Wiley. (d–g) Examples of TENG collecting water energy using FT working mode. (d) A tandem disk TENG (TD-TENG) for self-powered water quality monitoring. Illustration i–iv is the working schematic diagram. Reprinted with permission from Ref. [40]. Copyright 2019, Elsevier. (e) A fully symmetrical TENG based on an elliptical cylindrical structure (EC-TENG) composed of two coaxial elliptical cylindrical shells, where the inner TENG adopts a freestanding mode using a steel bar as the rolling element. Illustration i–iv is the working schematic diagram. Reprinted with permission from Ref. [80]. Copyright 2022, Springer Nature. (f) A graded energy harvesting TENG (GEH-TENG). Illustration i–iii is the working schematic diagram. Reprinted with permission from Ref. [81]. Copyright 2021, American Chemical Society. (g) A dual-mold TENG through an elastic-connection and soft-contact design. Illustration i–iv is the working schematic diagram. Reprinted with permission from Ref. [44]. Copyright 2021, Wiley.

It can be seen from the above analysis that FEC-TENG based on CS working mode has an outstanding contribution in collecting breeze energy. In particular, with the deepening of research, various dynamic models based on wind energy collection have been established, which is conducive to the further collection and utilization of energy.

With the help of wind cups, TENG-based wind energy harvesters can better harvest energy from the environment in FT mode. To collect different fluid energy, Xi et al. designed a new multi-functional TENG integrated by rotation TENG (r-TENG) and cylindrical TENG

(c-TENG), as shown in Figure 4e [7]. Both TENGs (r-TENG and c-TENG) are based on the FT working mode. r-TENG is designed to collect wind and water flow energy. The linear relationship between the short-circuit current of r-TENG and the applied wind speed is used for self-powered wind speed sensing devices. The integrated c-TENG can be used to collect water wave energy. The elastic rotation TENG designed by Zhang et al. adopts FT working mode and obtains appropriate mechanical contact at low pressure, which reduces the driving force [90]. Since the direct contact between the triboelectric layers causes serious wear on the surface of the material, in Figure 4f, Han et al. created a rotating TENG based on soft contact by using rabbit fur (SCR-TENG) [91]. The triboelectric material is composed of soft rabbit hair and polymer, and the FT working mode means that SCR-TENG has excellent triboelectric properties and super durability. Similarly, many FT-based TENGs use wind cups to drive and soft fur as triboelectric materials to collect wind energy in nature [31,92,93]. Moreover, a planetary rolling TENG is manufactured in rolling FT mode for simultaneous collection of wind energy and wind speed sensing [94]. The fluorinated ethylene propylene (FEP) film adheres to the surface of the roller to form the sliding part of the independent layer, thereby converting sliding friction into rolling friction (Figure 4g) [94]. Furthermore, the stability and durability of TENG based on the FT mode can be effectively improved by introducing a polymer film for charge replenishment into the non-contact FT structure. In Figure 4h, Lin et al. developed a pendulum-inspired TENG working in FT mode [83]. The PTFE films are set at the outer edge of the arc-shaped acrylic as the charge pump. In this working independent layer structure, there is a certain air gap (1 mm) between the slider and the stator [83]. Therefore, the slider (the pendulum) is very sensitive to external mechanical excitation, and a small disturbance leads to a large movement between the triboelectric layers. However, whether it is the use of an adaptive triboelectric layer or a soft triboelectric layer, the use of rod rolling instead of plane sliding, or the use of an additional triboelectric layer as a charge pump, wear will inevitably occur. At the same time, the non-contact structure leads to charge dissipation and reduces the output energy. Therefore, it is desirable to design FEC-TENG with the FT mode with excellent stability. With the help of the charge excitation strategy, in Figure 4i, Long et al. realized the increase in charge density of TENG in non-contact FT mode by self-excitation amplification between rotor and stator [42]. The high output of the floating self-excited sliding-TENG (FSS-TENG) enables it to continuously power small electronic devices in a weak wind of 3 m s^{-1} .

Therefore, the contact mode between the triboelectric materials of the device based on FT mode can be divided into direct contact [7] (Figure 4e), adding animal fur to form soft contact [91] (Figure 4f), changing sliding friction to rolling friction [94] (Figure 4g), and using additional friction material to supplement electric charge to form soft contact [83] (Figure 4h) and non-contact [42] (Figure 4i), etc. Regardless of the contact mode, the main purpose of these designs is to extend the durability of TENG based on the FT working mode and improve its energy collection efficiency and output performance at low wind speed.

From the above summary, we find that whether it is a water energy harvester or a wind energy harvester, TENG-based energy harvesters always tend to work in CS mode and FT mode. This is because CS-mode devices can be interestingly combined with most mechanical structures, expanding the energy harvesting range of TENGs. At the same time, the CS mode can effectively reduce the wear of the triboelectric layers and prolong the service life of the devices [87,88]. For the FT mode, the high collection efficiency always attracts a large number of researchers, and its excellent output performance continuously broadens the application scope of TENG [31,42]. Therefore, the above two working modes have irreplaceable positions in the energy harvesting field of TENG. However, most TENGs in LS mode and SE mode are used in signal acquisition and signal sensing, and they are not widely used in energy harvesting [95,96], so we will not discuss them here.

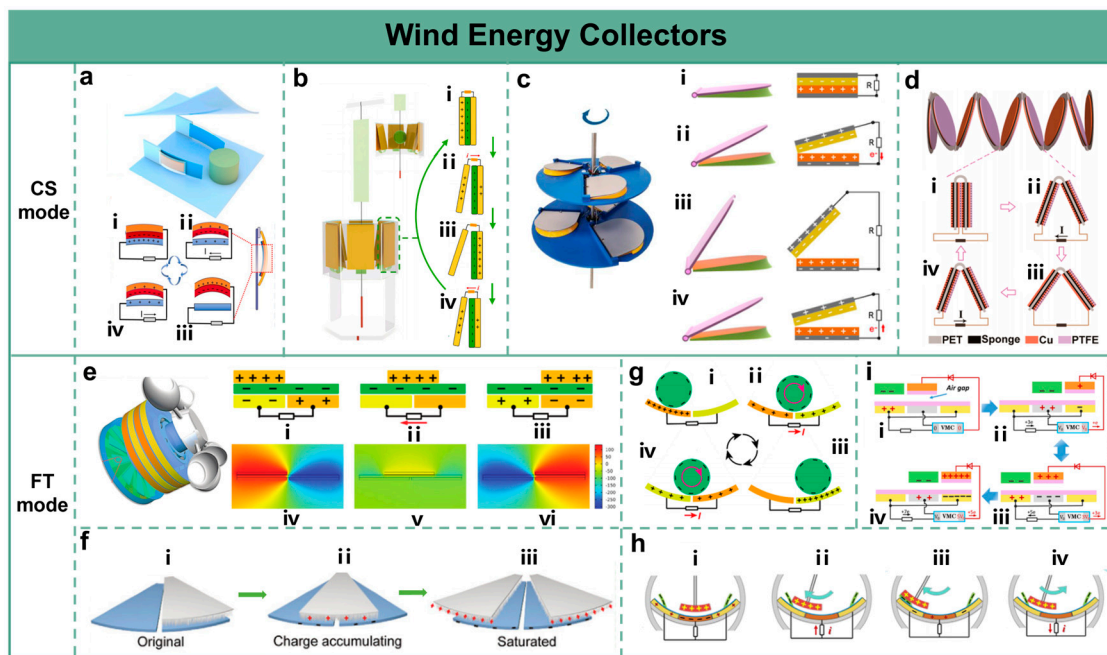


Figure 4. Systematic summary of TENG for collecting wind energy based on CS mode and FT mode working mode: (a–d) Examples of TENG collecting wind energy using CS working mode. (a) A novel TENG based on the wake galloping phenomenon using the minimalist CS mode. Illustration i–iv is the working schematic diagram. Reprinted with permission from Ref. [45]. Copyright 2022, Elsevier. (b) A TENG based on the flutter effect. Illustration i–iv is the working schematic diagram. Reprinted with permission from Ref. [6]. Copyright 2019, Springer Nature. (c) A new type of turbine disk-type TENG. Illustration i–iv is the working schematic diagram. Reprinted with permission from Ref. [85]. Copyright 2021, Elsevier. (d) Eight TENGs in CS mode connected in parallel to form the self-powered nitrogen oxide absorption and degradation system. Illustration i–iv is the working schematic diagram. Reprinted with permission from Ref. [89]. Copyright 2020, American Chemical Society. (e–i) Examples of TENG collecting wind energy using FT working mode. (e) Freestanding multifunctional TENG to harvest three types of energies including water waves, air flow, and water flowing. Illustration i–iii is the working schematic diagram. Illustration iv–vi is the potential simulation diagrams. Reprinted with permission from Ref. [7]. Copyright 2017, Wiley. (f) An improved rotary TENG using rabbit-hair-based soft-contact and FT mode. Illustration i–iii is the working schematic diagram. Reprinted with permission from Ref. [91]. Copyright 2022, Wiley. (g) A breeze-wind-driven autonomous wireless anemometer based on a planetary rolling TENG. Illustration i–iv is the working schematic diagram. Reprinted with permission from Ref. [94]. Copyright 2021, American Chemical Society. (h) A pendulum-inspired TENG operating at the FT mode. The problem of the charge dissipation in TENG of FT mode is well solved by using PTFE thin strip as a triboelectric layer. Illustration i–iv is the working schematic diagram. Reprinted with permission from Ref. [83]. Copyright 2019, Elsevier. (i) A floating self-excited sliding TENG formed by self-excited amplification between the rotor and the stator. Illustration i–iv is the working schematic diagram. Reprinted with permission from Ref. [42]. Copyright 2021, Springer Nature.

However, whether it is a wind energy harvester or a water energy harvester, we need to collect enough energy through them. Therefore, only focusing on the structural design cannot effectively improve the performance output and energy harvesting efficiency of FEC-TENG. At the same time, the low energy output also hinders the practical application based on FEC-TENG. So how to efficiently harvest environmental mechanical energy? How to judge the efficiency of the FEC-TENG? In what ways can the efficiency of the collectors be improved? We will answer these questions below.

3. Theoretical Analysis and Application Examples in the Energy Transfer Process of FEC-TENGs

By studying the energy conversion process and kinetic characteristics of FEC-TENG, we can further improve the energy conversion efficiency and performance output of FEC-TENG from different stages of the energy conversion process.

Based on most studies focusing on the design and optimization of the structure of FEC-TENGs, the energy transfer process of FEC-TENGs is mainly divided into four processes in the process of capturing and utilizing energy from the natural environment [36]. As shown in Figure 5a, firstly, FEC-TENGs collect fluid energy from the environment, called overall mechanical energy, with an energy conversion efficiency of η_1 . However, the overall mechanical energy cannot be fully utilized by the TENG units. For example, wind or water in nature always triggers the package shell or triggers the end of FEC-TENG first, and then the package shell and trigger end will harvest part of the energy and transfer it to the working unit of TENG. This part of the energy, we call the available mechanical energy captured by the working module, with an energy conversion efficiency of η_2 . Then, the working unit of TENG converts the obtained mechanical energy into electrical energy by coupling triboelectrification and electrostatic induction effects [5], with an energy conversion efficiency of η_3 . Finally, through signal processing or energy management, FEC-TENGs become self-powered sensors or the power supply for small electronic devices. Therefore, we define the energy conversion efficiency η of FEC-TENG consists of three parts, namely, η_1 , η_2 , and η_3 .

$$\eta = \eta_1 \cdot \eta_2 \cdot \eta_3, \tag{3}$$

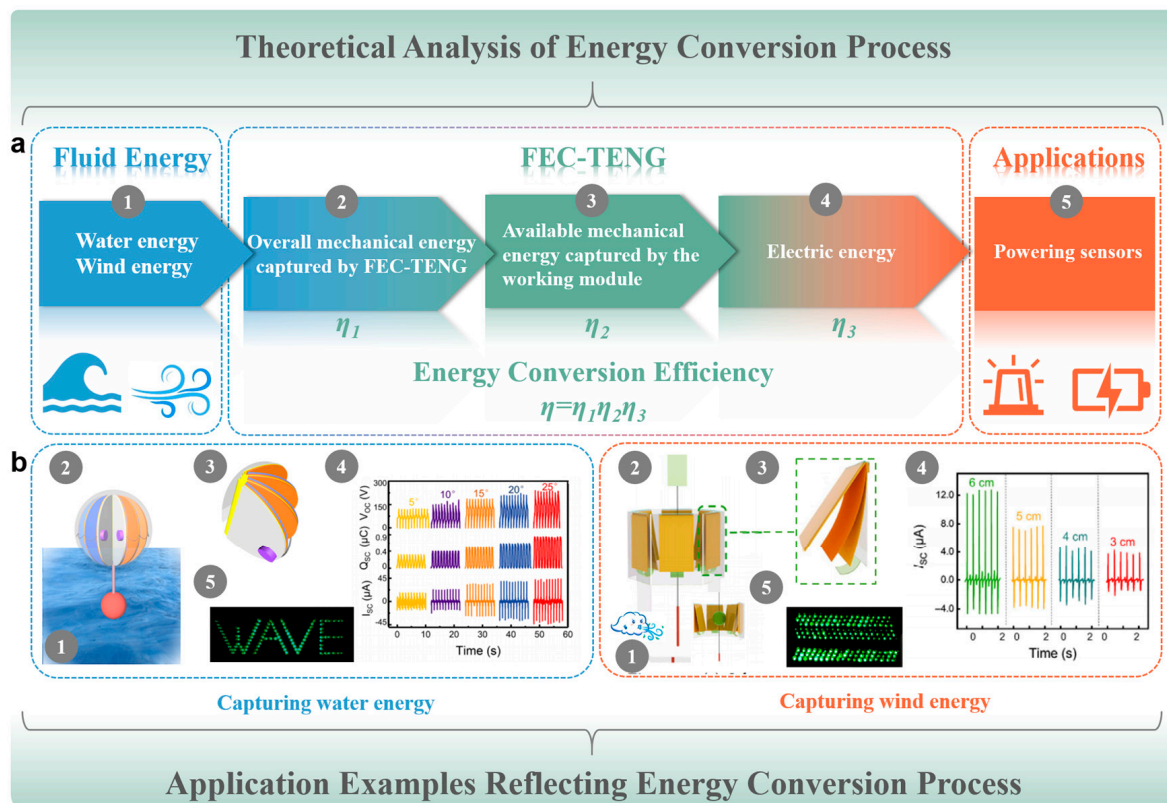


Figure 5. Theoretical analysis and application examples of energy conversion in the process of TENG collecting fluid energy: (a) Theoretical analysis of energy conversion process and calculation of energy conversion efficiency. (b) Application example of energy conversion process based on collecting water and wind energy. Reprinted with permission from Ref. [6]. Copyright 2019, Springer Nature. Reprinted with permission from Ref. [36]. Copyright 2022, Elsevier.

However, through literature research, we found that most FEC-TENGs ignore the calculation of conversion efficiency η_1 and η_2 when calculating the conversion efficiency η , so the calculated results are not accurate [36]. Next, two application examples are introduced to accurately reflect the theoretical analysis of the above energy conversion process [6,36]. As for capturing the water energy, an inverted pendulum multi-layer TENG (IPM-TENG) developed by Zhang et al. can fully demonstrate the above energy conversion process [36]. Firstly, IPM-TENG vibrates with water waves, and its floating body and assisting body capture part of the mechanical energy of water. Then, the floating body and the assisting body transfer the captured mechanical energy to the working unit of IPM-TENG. Finally, the TENG unit inside the IPM-TENG works and outputs power to complete the conversion from mechanical energy to electrical energy. The energy conversion efficiency η_1 and η_2 of the two-body mode IPM-TENG is 0.34% and 12.98%, respectively. And the energy conversion efficiency η_3 of the two-body mode IPM-TENG is 14.5%. Therefore, the energy conversion efficiency η of the two-body mode IPM-TENG is 0.0064%.

At present, a large number of studies focus on improving η_3 , while ignoring η_1 and η_2 . However, the application example of IPM-TENG capturing water wave energy reveals that increasing η_1 , η_2 , and η_3 can effectively improve the total energy conversion efficiency η of FEC-TENGs. Excitingly, Xu et al. studied the interaction between floating structures and water waves in FEC-TENGs that collect water energy and revealed the law of wave–structure interaction [97]. The results show that the cubic shell has the highest absorbing ability, and the wave response ability of the spherical shell is positively correlated with the wave intensity, the diameter of the spherical shell, and the height of the center of mass [97]. With the increase in weight, the wave response ability of the spherical shell decreases first and then increases slightly [97]. From the perspective of energy conversion, this work points out the direction of the structural design of the future efficient FEC-TENG, which has important guiding significance for the acquisition of blue energy.

As for capturing the wind energy, FE-TENG designed by Hu et al. is representative in demonstrating the energy transfer process [6]. In Figure 5b, the PET tape on the FE-TENG swings around with the wind, capturing some mechanical energy from the wind. Then, the swinging PET tape drives the silicon ball under the PET tape, and the silicon ball transfers part of the captured mechanical energy to the working unit of FE-TENG through impact [6]. Finally, the working unit outputs electrical signals to complete the energy conversion. Although the author did not carefully calculate the energy conversion efficiency of each part, the energy conversion process of FE-TENG and IPM-TENG is highly similar, which is consistent with our theoretical analysis. However, due to the complex calculation process, the output efficiency of most FEC-TENGs is not calculated. Therefore, we intend to use the below performance parameters to indirectly reflect the efficiency of the FEC-TENGs.

Some necessary parameters can reasonably evaluate the output performance of FEC-TENGs [98]. Common basic output parameters include short-circuit charge Q_{SC} , short-circuit current I_{SC} , open-circuit voltage V_{OC} , output power P , and average power \bar{P} . Moreover, because FEC-TENGs have different structural designs and sizes, it is more accurate to use peak power density and average power density to compare the output performance of the devices [98]. Furthermore, considering that FEC-TENGs are mostly used in the collection of breeze energy and wave energy, the minimum working frequency, the output stability, and the packaging state of the device should also be taken into account. To promote the commercialization of FEC-TENGs, we will compare the matching impedance of FEC-TENGs and consider whether they can be networked. To compare the performance of each FEC-TENG more comprehensively, therefore, we add the output power area density ρ_{SP} , output power volume density ρ_{VP} , average power area density ρ_{ASP} and average power volume density ρ_{AVP} , minimum working frequency f_{min} , stability, matching impedance R , encapsulation state, and the state of networking to further evaluate each

device. Assuming that S is the electrode area and V is the volume of the device, then ρ_{SP} , ρ_{VP} , ρ_{ASP} , and ρ_{AVP} are defined as follows:

$$\rho_{SP} = \frac{P}{S}, \quad (4)$$

$$\rho_{VP} = \frac{P}{V}, \quad (5)$$

$$\rho_{ASP} = \frac{\bar{P}}{S}, \quad (6)$$

$$\rho_{AVP} = \frac{\bar{P}}{V} \quad (7)$$

So far, we have described and introduced the energy conversion process and performance parameters of FEC-TENGs in detail. In the research of FEC-TENGs in recent years, a large number of excellent works have shown the broad prospects of collecting fluid energy, and we will introduce them in the following categories.

4. Structural Design and Performance Evaluation of FEC-TENGs

Considering that FEC-TENGs have a variety of structural design and energy collection methods, we will review FEC-TENGs based on the CS mode and FT mode in the following chapters from the aspects of device packaging, energy transfer process, and collection of unidirectional water energy or omnidirectional water energy.

4.1. FEC-TENGs Based on CS Mode for Collecting Single-Direction Water Energy

Based on the CS mode, the working unit structures of FEC-TENGs are very simple, and they can produce good output even at a small driving frequency. Moreover, the device structure of such FEC-TENGs can be divided into a non-encapsulated mode and a fully encapsulated mode. The non-encapsulated FEC-TENGs avoid direct contact between the device and water in the process of collecting water energy and also reduce the difficulty of packaging in the process of device fabrication. Here, based on the pendulum-like structure design, a non-encapsulated hybrid nanogenerator was made [59]. Through ingenious structural design, the generator successfully combines three parts: TENG, EMG, and solar cell, as shown in Figure 6a. Moreover, the combination of TENG and EMG broadens the operating frequency range of the hybrid generator, enabling it to better collect water wave energy below 2 Hz [59]. Better still, the integration of solar panels can effectively increase the power supply and improve the volume utilization of the equipment. The output of these three generators is shown in Figure 6b. Driven by water waves, the short-circuit currents of TENG and EMG are 34 μA and 3.5 mA, and the open-circuit voltages are 491 V and 1.74 V, respectively [59]. The solar panel can produce an output of 72.5 mA and 6.9 V. Since this is only a review of the fluid energy collected by TENG, we only list and compare the output performance of TENG. When the four TENG working units in the hybrid nanogenerator are connected, the TENG units generate a current output of 41.3 μA and a voltage output of 567 V at a working frequency of 1.25 Hz. The minimum response frequency of the TENG is 0.25 Hz, and its stability can reach 100% (800,000 cycles). When the matching impedance is 60 M Ω , the peak power density of the TENG is 0.5625 W m⁻² Hz⁻¹. Coincidentally, in Figure 6c, a non-encapsulated polymorphous U-shaped TENG (NPU-TENG) was designed [95]. With three trigger terminals, NPU-TENG can collect water wave, water flow, and raindrop energy, and its peak power density reaches 1.97 W m⁻³ Hz⁻¹. However, although the non-encapsulated structure can effectively eliminate electrostatic shielding and material corrosion in water, the structure relies on additional supports and platforms. The design of the trigger end further reduces the output efficiency. Therefore, the research on the packaging structure is more systematic.

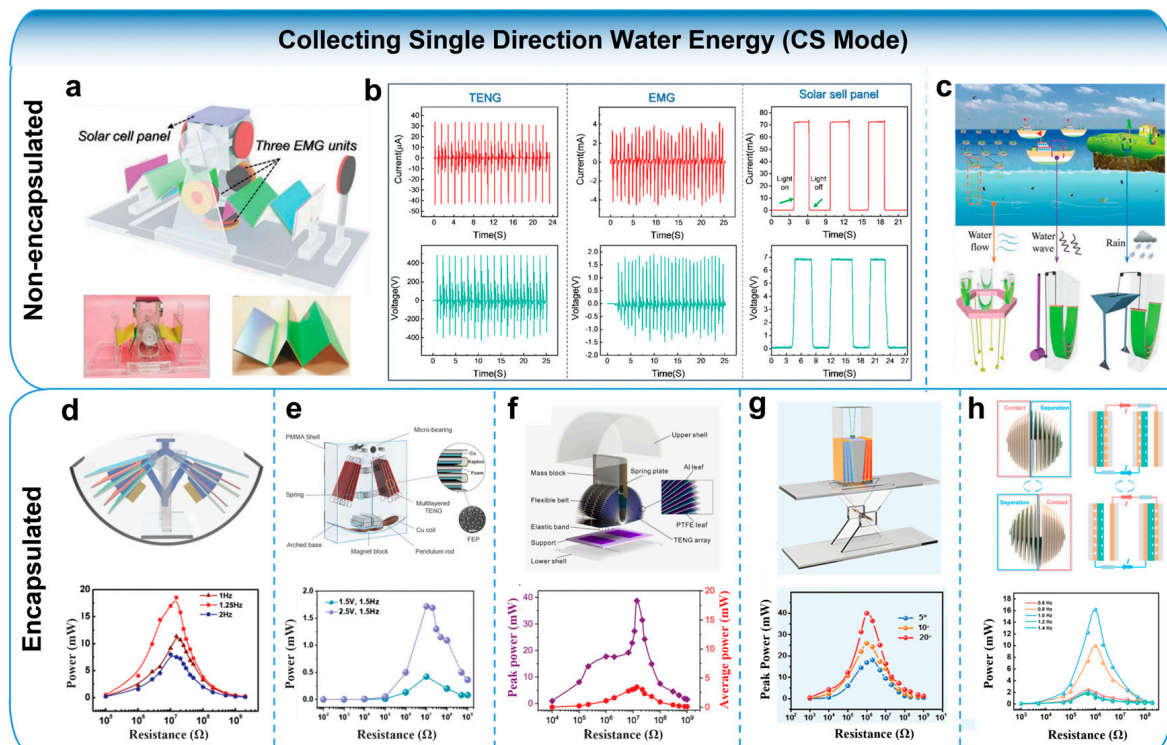


Figure 6. Structure and performance of TENG based on CS mode for collecting single-direction water energy: (a,b) A non-encapsulated pendulum paper-based hybrid nanogenerator for multi-energy collection. Reprinted with permission from Ref. [59]. Copyright 2019, Wiley. (c) Non-encapsulated U-shaped TENG. Reprinted with permission from Ref. [95]. Copyright 2021, Wiley. (d) Butterfly-inspired TENG with spring-assisted linkage. Reprinted with permission from Ref. [99]. Copyright 2021, Wiley. (e) Pendulum hybrid wave energy harvesting nanogenerator based on spring-assisted multilayer structure. Reprinted with permission from Ref. [58]. Copyright 2021, Wiley. (f) Open-book-like TENG based on roll-swing oscillators. Reprinted with permission from Ref. [100]. Copyright 2019, Royal Society of Chemistry. (g) A double-pendulum coupled hybrid nanogenerator (BCHNG) module integrated into a ship-like platform to collect wave energy. Reprinted with permission from Ref. [101]. Copyright 2022, Wiley. (h) Multilayered helical spherical TENG with charge shuttling. Reprinted with permission from Ref. [102]. Copyright 2023, Wiley.

To collect water wave energy, a butterfly-inspired TENG (B-TENG) with a spring-assisted four-bar structure was developed (Figure 6d) [99]. The spring-assisted structure can stimulate the multiple contact separation of the TENG working module so that it can obtain energy from different types of low-frequency waves. At 1.25 Hz, B-TENG achieves an output of 75.35 μA and 707.01 V. Its maximum average output power density is as high as 7.65 $\text{W m}^{-3} \text{Hz}^{-1}$ (9.559 W m^{-3}) and it can easily light up 180 LEDs. Furthermore, with different device placement methods, the device obtains multi-directional water wave energy from different types of motion. Similarly, with the help of a spring-assisted multilayer structure, in Figure 6e, Ren et al. mixed TENG and EMG to design a pendulum-type wave energy harvesting nanogenerator (HW-NG) [58]. Its minimum driving frequency can reach 0.5 Hz, and the peak power density can reach 0.273 $\text{W m}^{-2} \text{Hz}^{-1}$. And HW-NG can be effectively networked to realize the transmission of early warning signals per second at sea. To further improve the output energy density of such TENGs, Zhong et al. efficiently integrated a large number of TENG units into an open-book-like structure in a limited space, and made an open-book-like TENG (OB-TENG) [100], as shown in Figure 6f. For the first time, OB-TENG proposes a force conduction chain structure to effectively drive multiple stacked TENG units [100]. For a device consisting of 50 units, it can output a short-circuit current of 450 μA and a charge of 26 μC at a driving frequency as low as

1.15 Hz. Its minimum driving frequency is as low as 0.2 Hz. Most importantly, the peak power density of OB-TENG reaches $9.675 \text{ W m}^{-3} \text{ Hz}^{-1}$, and the average power density is $0.863 \text{ W m}^{-3} \text{ Hz}^{-1}$. Similarly, in Figure 6g, based on the integration of multi-layer CS-mode TENG, Zhang et al. made a bifilar-pendulum coupled hybrid nanogenerator (BCHNG) module integrated on a ship platform [101]. With the motion of the ship's flap and the swing of the double pendulum, BCHNG can simultaneously collect low-frequency ocean waves with kinetic energy and gravitational potential energy, which greatly increases the output power of the TENG module in the system. Remarkably, the TENG module in BCHNG can generate a current of $700 \mu\text{A}$ at a driving frequency of 2 Hz, and its peak output density and average power density are as high as 196 W m^{-3} and 5.7 W m^{-3} , respectively [101]. As for improving the space utilization of the energy harvesting device, a spherical TENG (MH-TENG) with multi-layer spiral units (Figure 6h) was fabricated as well [102], and its space utilization rate reached 92.5%. Based on the charge shuttle mechanism, the peak power density of a single TENG is as high as $23.2 \text{ W m}^{-2} \text{ Hz}^{-1}$.

In summary, based on the CS mode, the FEC-TENGs that collect unidirectional water energy can effectively improve the space utilization efficiency of the device and increase the peak power density and average power density by using the laminated structure. However, most of these common laminated structure designs in the literature only collect water energy in a single direction, which is not conducive to improving the energy conversion efficiency η_1 . Moreover, as shown in Figure 6g, the analysis of the energy conversion process more effectively improves the output power of the device, which coincides with our previous analysis. Therefore, in the following review, we will further use typical examples to analyze the energy conversion process of FEC-TENGs in omnidirectional water energy collection.

4.2. FEC-TENGs Based on CS Mode for Collecting Omnidirectional Water Energy

In the natural environment, the direction of motion of wave energy or water energy is variable. Therefore, only collecting water energy in a single direction is not enough for FEC-TENGs based on CS mode. Moreover, it is necessary to deeply analyze the energy conversion and the dynamic behavior of the device during the collection process. An et al. constructed a whirling-folded TENG (WF-TENG) using 3D printing and printed circuit board technology, and its flexible vortex structure responds well to various forms of wave excitation [103]. In the process of collecting omnidirectional water energy, WF-TENG can produce a peak power density of $8.86 \text{ W m}^{-3} \text{ Hz}^{-1}$. Moreover, Zhang et al. studied an active resonant TENG (AR-TENG) system [37]. As shown in Figure 7a, the system can collect water wave energy in all directions through good structural design and resonance effect. In Figure 7b, the author introduces in detail the role of the single pendulum, tumbler, and flexible ring TENGs in capturing ocean energy and output energy in the AR-TENG system. Finally, the peak power density of AR-TENG reached 4.59 W m^{-3} (Figure 7c). Based on the theory of fluid mechanics, Zhang et al. revealed the energy conversion mechanism and interaction mechanism between IPM-TENG and water waves (Figure 7d) [36]. The optimized IPM-TENG has an available energy conversion efficiency η_3 of 14.5% and an average power density of $3.15 \text{ W m}^{-3} \text{ Hz}^{-1}$ (Figure 7e). Similarly, based on computational fluid dynamics (CFD), Wang et al. analyzed the blade shape and number parameters of the self-made bionic butterfly wings TENG (BBW-TENG) in Figure 7f–h and verified that the bionic blade had resistance amplification characteristics [104]. Under multi-directional water wave excitation, the minimum response frequency of BBW-TENG is as low as 0.1 Hz, and its electrical performance is still not reduced after 45 days of immersion in water.

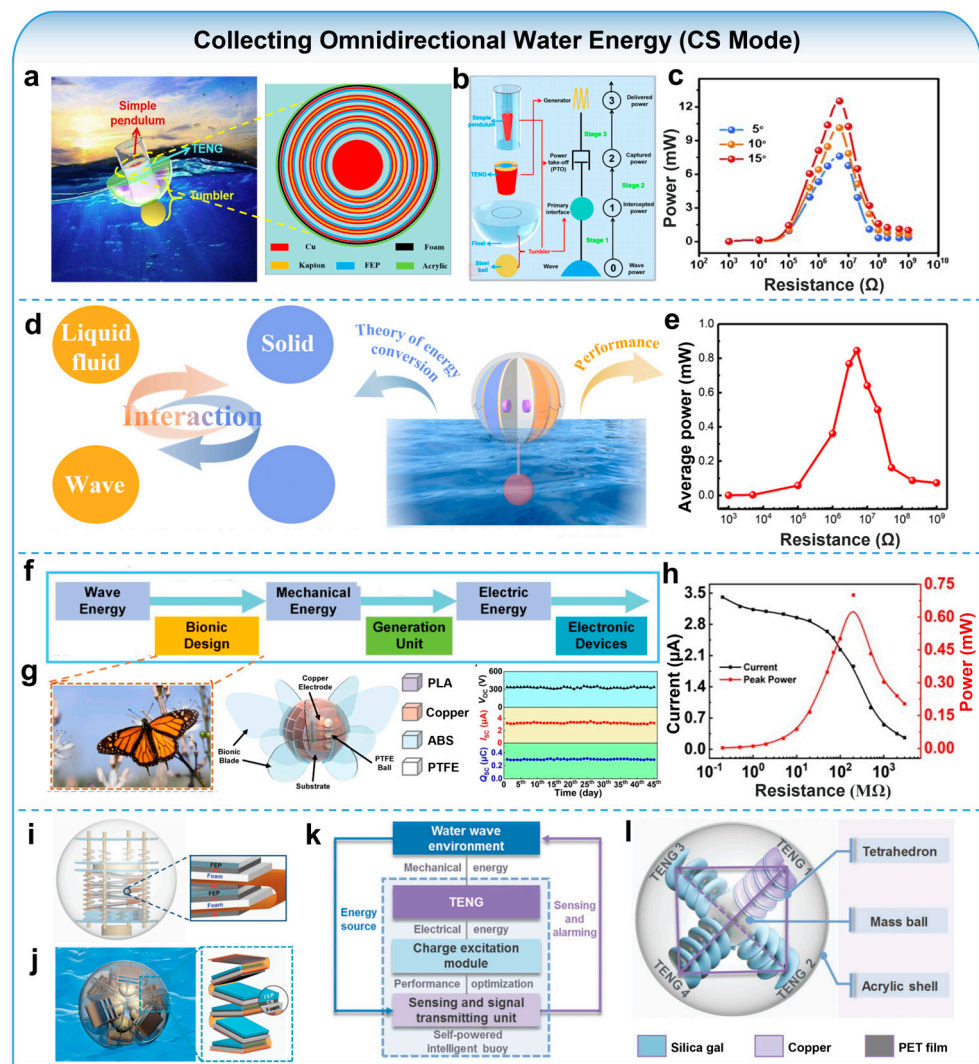


Figure 7. Structure, energy conversion process, and performance of TENG based on CS mode for collecting omnidirectional water energy: (a–c) An active resonance TENG (AR-TENG) system fabricated by using the simple pendulum, the tumbler, and the flexible ring. Reprinted with permission from Ref. [37]. Copyright 2021, Elsevier. (d,e) An inverted pendulum-typed multilayer TENG (IPM-TENG). Reprinted with permission from Ref. [36]. Copyright 2022, Elsevier. (f–h) A butterfly-winged TENG (BBW-TENG) for collecting multidirectional wave energy from underwater environments. Reprinted with permission from Ref. [104]. Copyright 2022, Elsevier. (i) A spherical TENG unit based on a spring-assisted multilayer structure and integrated power management module (PMM). Reprinted with permission from Ref. [105]. Copyright 2019, Wiley. (j) A spherical TENG with a spring-assisted multilayer structure for collecting water wave energy from multiple trigger directions. Reprinted with permission from Ref. [78]. Copyright 2020, Royal Society of Chemistry. (k,l) A self-powered intelligent buoy for TENG energy harvester through water wave energy conversion in water disaster alarm system. Reprinted with permission from Ref. [35]. Copyright 2022, Wiley.

It has to be mentioned that effective power management schemes are essential for the large-scale collection of blue energy. Liang et al. have conducted very systematic work in this area. First, as shown in Figure 7i, they used a spring-assisted multi-layer spherical TENG unit to form a hexagonal TENG network for collecting multiphase water wave energy [105]. The author integrates the rectifier bridge, switch, parallel free-turn diode D, parallel inductance L, parallel capacitance C, and other components into a classic AC/DC step-down conversion circuit [105]. The current output of the TENG can reach 270 μA at a driving frequency of 1 Hz. Then, the author further improves the TENG by integrating six

identical unit structures into a spherical shell, as shown in Figure 7j. The optimized TENG increases the charging speed of the supercapacitor by 100 times [78]. Finally, in Figure 7k,l, they designed a spherical TENG device with four spiral units to collect omnidirectional water energy, and integrated charge excitation modules (CEMs) to improve its power output [35]. It is gratifying that the spherical TENG with CEMs generates an output current of up to 15.09 mA at a driving frequency of 1.2 Hz. At present, there are many examples of using energy management circuits and charge excitation modules to further improve the efficiency of FEC-TENGs for collecting water energy [106–109]. In addition, Deng et al. adopted a novel gas exchange structure and a rigid/flexible coupling deformation mechanism to ensure that the high-performance paired TENG can work effectively in deep-water high-pressure environments [77]. The TENG can be integrated into the thin flexible layer on a large scale and has great potential in the utilization of water flow energy.

In summary, FEC-TENGs based on CS mode have gradually developed from collecting water energy in a single direction to collecting water energy in all directions. The structure of the device has developed from a simple design to the need to combine theoretical analysis, and now it is necessary to establish a suitable fluid mechanics model. At the same time, based on the research on the energy conversion process, the research of FEC-TENGs based on the CS mode for collecting water energy is very representative and has achieved good results. The summary of the output performance of these devices is shown in Table 1.

4.3. FEC-TENGs Based on FT Mode for Collecting Water Energy

Compared with the CS working mode, FEC-TENGs based on the FT working mode have higher efficiency in collecting water energy. Combined with a variety of design structures, FEC-TENGs based on FT mode have greater energy output and richer practical applications.

As shown in Figure 8a, Bai et al. designed a high-performance tandem disk TENG (TD-TENG) for self-powered water quality detection [40]. The peak power density of TD-TENG reaches $7.89 \text{ W m}^{-3} \text{ Hz}^{-1}$, with an average power density of $2.24 \text{ W m}^{-3} \text{ Hz}^{-1}$. At a driving frequency of 0.58 Hz, the output current of TD-TENG is as high as $675 \mu\text{A}$. However, this type of TENG will undergo excessive rotation or overturning under extreme ocean conditions, which hinders the further utilization of ocean energy. Therefore, in Figure 8b, combining CS-TENG and FT-TENG, a fully symmetric TENG with an elliptical cylinder swing structure (EC-TENG) was designed [80]. Thanks to the completely symmetrical structure design, even if it is overturned by rough waves, EC-TENG can still work normally and its output will not decrease. With the help of a turbine, in Figure 8c, an easy-to-assemble hybrid nanogenerator (EANG) can be used to collect fluid energy [43]. The encapsulation, maintenance, and assembly of EANG become easier due to the introduction of magnetic coupling, which further promotes the commercialization of fluid energy harvesting. In addition, in Figure 8d, using the connecting rod structure, the unidirectional rotating TENG based on rabbit hair (WLM-TENG) shows us a variety of self-powered applications, including energy supply for indicator LEDs, multifunctional barometers, portable anemometers, and multifunctional water quality detection pens [110]. Although the above FEC-TENGs based on FT mode have improved performance compared with FEC-TENGs based on CS mode, they can only collect fluid energy acting on the direction of the working unit. For the collection of fluid energy in any direction, the design and performance of FEC-TENGs are as follows.

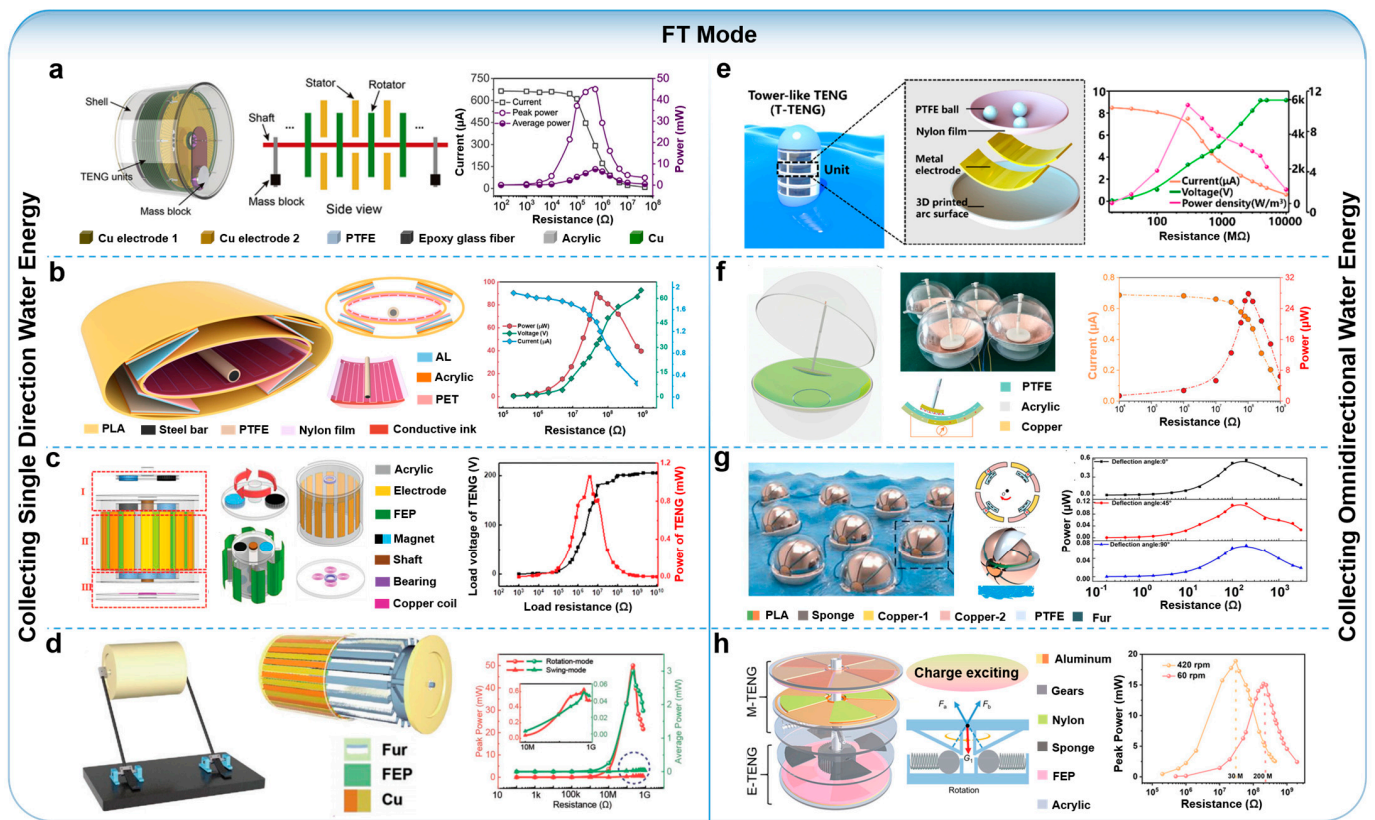


Figure 8. Structure and performance of TENG based on FT mode for collecting water energy: (a–d) TENG for collecting single-direction water energy. (a) A tandem disk triboelectric nanogenerator (TD-TENG) with a radial grating structure. Reprinted with permission from Ref. [40]. Copyright 2019, Elsevier. (b) A fully symmetrical TENG based on an elliptical cylindrical structure (EC-TENG). Reprinted with permission from Ref. [80]. Copyright 2022, Springer Nature. (c) An easily assembled electromagnetic-triboelectric hybrid nanogenerator driven by magnetic coupling. A magnetic coupling (I), a sliding freestanding mode TENG (II) and an EMG (III) Reprinted with permission from Ref. [43]. Copyright 2019, Wiley. (d) A cylindrical wave-driven linkage mechanism TENG (WLM-TENG) with unidirectional rotation. Reprinted with permission from Ref. [110]. Copyright 2023, Wiley. (e–h) TENG for collecting omnidirectional water energy. (e) A design of high-power density TENG based on a tower structure (T-TENG). Reprinted with permission from Ref. [111]. Copyright 2019, American Chemical Society. (f) An elastic-connection and soft-contact TENG (ES-TENG) with a pendulum-like structure. Reprinted with permission from Ref. [44]. Copyright 2021, Wiley. (g) A gyroscope-structured TENG (GS-TENG). Reprinted with permission from Ref. [41]. Copyright 2022, American Chemical Society. (h) A rotational TENG enabled by automatic mode switching and charge excitation (CEMA-TENG). Reprinted with permission from Ref. [112]. Copyright 2022, Wiley.

In Figure 8e, the tower-shaped TENG (T-TENG) composed of PTFE balls and nylon film coated on the three-dimensional printed curved surface has a high-power density [111]. Based on the power generation model and dynamic model of T-TENG, it is found that the power density of T-TENG increases with the increase in the number of units [111]. The power density of T-TENG increases linearly from 1.03 W m^{-3} to 10.6 W m^{-3} with the increase in the unit number from 1 to 10. Inspired by the pendulum structure, Lin et al. made a super-robust and frequency-multiplied TENG (P-TENG) for collecting all-around fluid energy [44,83]. The P-TENG converts the impact kinetic energy brought by the fluid into potential energy, which greatly improves the collection efficiency. At the same time, using PTFE strips as charge supplement materials, P-TENG has ultra-high sensitivity and excellent durability for long-term operation [83]. Next, they introduced spring and flexible dielectric fluff into the P-TENG to form an elastically connected soft-contact TENG (ES-

TENG) [44], as shown in Figure 8f. Through the above ingenious design, the friction charge on the surface of the pendulum is supplemented, the efficiency of ES-TENG is doubled, and the energy conversion efficiency is as high as 29.7%. Also benefiting from animal fur, the segmented swing TENG (SSF-TENG) designed by Pang et al. reduces the frictional resistance and material wear between the triboelectric layers [82]. In Figure 8g, a TENG based on a gyroscope structure (GS-TENG) uses animal fur as the friction layer. At the same time, its internal and external power generation units operate independently in different directions, realizing the collection of multi-directional wave energy [41]. Additionally, in Figure 8h, Fu et al. made a rotary TENG using automatic mode switching and charge excitation strategies (CEMA-TENG) [112,113]. CEMA-TENG not only maintains 94% output performance after 72,000 cycles but also can power LEDs, infrared light alarm modules, and thermometers by collecting high-speed fluid energy. More amazingly, recently, inspired by mechanical metamaterial structures, Li et al. designed a new type of 3D chiral TENG network to collect wave energy in all directions [114]. The unbalanced unit of chiral connection endows the network with flexibility, and superelasticity in water and wave absorption behavior. Combined with the power management circuit, the area peak power density of the TENG network is 5066 W m^{-2} , and the volume peak power density is $31,665 \text{ W m}^{-3}$.

In summary, most of the research on FEC-TENGs based on FT mode not only ensures high output performance but also focuses on improving the wear resistance of the rotating structure and the sensitivity to external driving [115–117]. By combing the research of FEC-TENGs based on collecting water energy, we find that whether it is based on the CS mode or FT mode, analyzing and optimizing the energy collection process in stages can effectively improve the output performance of the devices [35–37]. In addition, the detailed performance comparison of FEC-TENGs for collecting water energy is shown in Table 1.

4.4. Structure and Performance of FEC-TENGs for Collecting Wind Energy

Unlike FEC-TENGs that collect water energy, FEC-TENGs that collect wind energy have few requirements for device packaging. The main research focuses on how to efficiently collect wind energy and how to reduce the wear between the triboelectric layers. Next, we will introduce the performance of FEC-TENGs based on the CS mode and FT mode when respectively collecting wind energy.

In Figure 9a, based on the flow-induced vibration effect, a CS-mode TENG (FIV-TENG) to collect low-speed wind energy was designed [38]. Since the TENG unit is encapsulated in a bluff body and connected to a cantilever beam, the power generation unit is separated from the wind drive unit to avoid the huge rotational resistance and friction and wear of the ordinary wind energy harvester. However, the minimum operating wind speed of FIV-TENG is 2.9 m s^{-1} , and its output performance needs to be improved. Heo et al. developed a TENG based on charge accumulation flutter (CAF-TENG), which has ultra-high root mean square current (36 mA) and average power density (26 mW cm^{-3}) [118]. By introducing a flutter conductive layer, a charge-induced layer, and a fixed electrode with a discharge channel structure, CAF-TENG can efficiently collect the energy of the respiratory airflow and play a role in respiratory monitoring or real-time safe lighting. In Figure 9b, based on the above structure, Son et al. added the ambient air ionization channel (AAIC) to improve the output performance of the flutter-driven TENG based on charge polarization (CPF-TENG) [119]. It is gratifying that the device can generate peak voltage and current outputs of 2000 V and 4 A. At the same time, a large number of CPF-TENGs are connected in series to collect omnidirectional breeze wind energy [119]. In Figure 9c, based on the CS working mode, a simple, low-cost, transparent, and fully bendable ambient wind energy harvester was proposed [120]. By integrating multiple units, the lawn-structured TENG can easily collect multi-directional wind energy. At the same time, the integrated device of multiple units is installed on the roof of a model room. The environmental wind energy obtained by the TENG can be used to illuminate the advertising display board [120]. Similarly, in Figure 9d, based on the FIV effect and fluid mechanics theory, Zhang et al. established a dynamic model of mechanical energy and electrical energy conversion and

designed the F-TENG [39]. Because F-TENG can collect multi-directional wind and drive some commonly used electronic devices, the author constructed an intelligent fire detection system to provide data support for reducing fire risk. It can be seen that FEC-TENGs based on CS working mode can generally achieve multi-directional wind energy collection through simple unit overlap in the process of collecting wind energy [6,39,45,118]. At the same time, the analysis of energy conversion and dynamic processes in the process of wind energy collection is helpful to further improve the output performance of this kind of TENG [39].

However, with the help of the wind cup, the FEC-TENG based on the FT mode is more adept at harvesting wind energy. A large number of studies have proved that FEC-TENGs based on FT mode have better output performance when collecting wind energy [121–123]. Here, we divide the FT-based FEC-TENGs into the following four categories, direct-contact mode, soft-contact mode, non-contact mode, and solid–liquid-contact mode. In Figure 9e, Xi et al. designed a common multifunctional TENG based on FT mode [7]. As a typical representative of FT mode FEC-TENGs, the average power density of this multifunctional TENG is 0.034 W m^{-2} . To reduce the wear and friction between the triboelectric layers, in Figure 9f, a rabbit-hair-based rotary TENG using soft contact (SCR-TENG) was developed [91]. The soft rabbit hair improves the stability of the device. It was found that the output performance of SCR-TENG did not change during the stability test of more than 480,000 cycles. Moreover, the electromechanical energy conversion efficiency of SCR-TENG reaches 15.4%. Additionally, this method of using the soft fur as the triboelectric layers to improve the stability of FT-mode TENG has been adopted by many researchers and achieved good results [31,93,124,125]. Based on the charge excitation and air breakdown model, in Figure 9g, Long et al. designed a floating sliding TENG (FSS-TENG) that achieves self-enhancement of charge density through self-excited amplification between the rotor and the stator [42]. Since the rotor and stator are non-contact modes, the FSS-TENG still maintains 100% performance output after more than 100,000 cycles [42]. The research of FSS-TENG is of great significance to the development of capturing micromechanical energy. However, the electrodes exposed to the air make FSS-TENG more likely to have air breakdown or dielectric breakdown, which is unfavorable for TENGs that use non-contact mode to collect wind energy. Therefore, in Figure 9h, the self-excited liquid suspension TENG (LS-TENG) was developed [126]. By systematically studying the charge transport behavior in dielectric liquids, the output performance of LS-TENG is effectively improved, and it has the advantages of small driving force, long life, and high energy conversion efficiency [126]. At a wind speed of 3 m s^{-1} , the rotating LS-TENG can charge a 10 mF capacitor to 6 V in 80.5 s with the help of power management, demonstrating the outstanding ability of LS-TENG to collect wind energy.

At present, FEC-TENGs for collecting wind energy have good development prospects. Whether it is collecting high-speed wind energy or low-speed wind energy, FEC-TENGs have been greatly improved in performance output, stability, and electromechanical conversion efficiency.

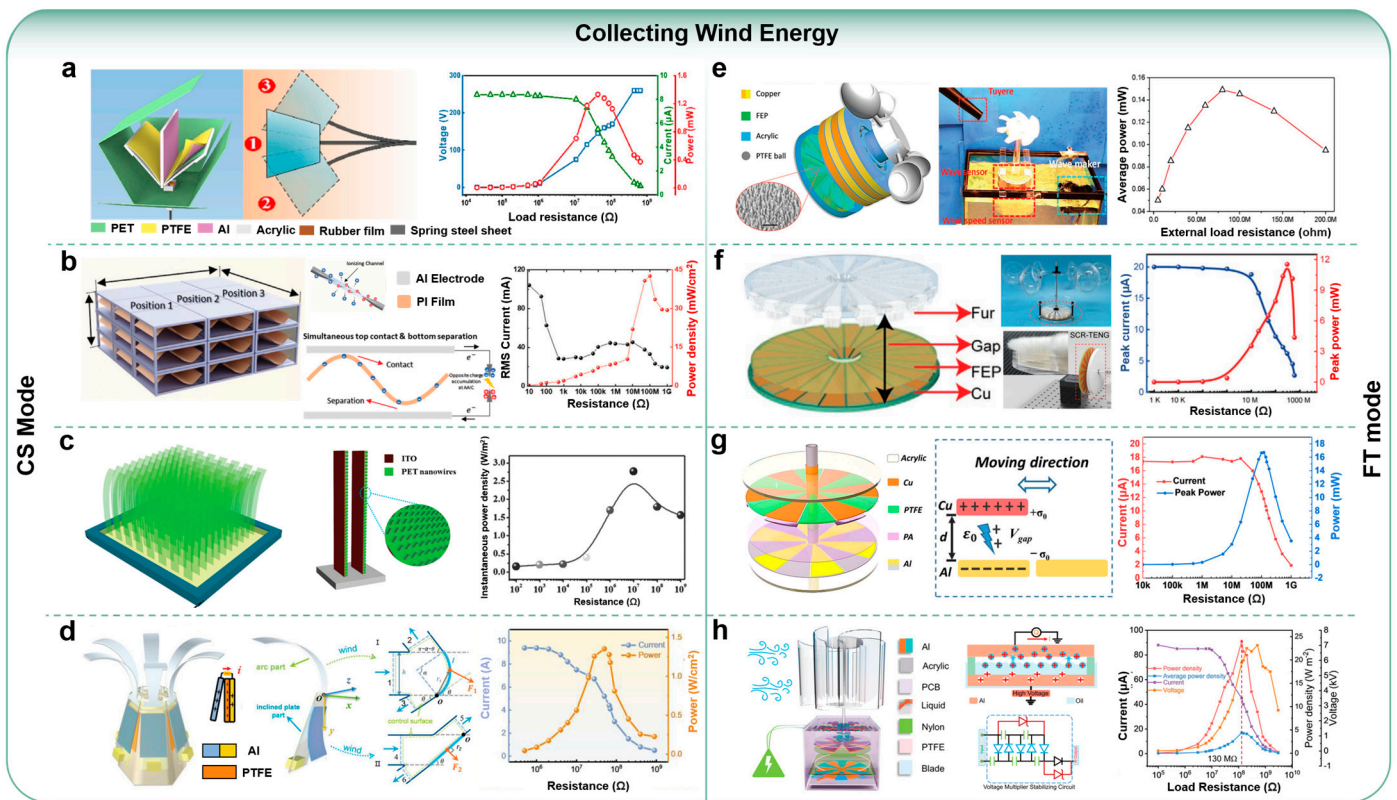


Figure 9. Structure and performance of TENG for collecting wind energy: (a–d) TENG based on CS mode. (a) A full-packaged TENG based on flow-induced vibration effect (FIV-TENG). Reprinted with permission from Ref. [38]. Copyright 2020, Elsevier. (b) A charge-polarization-based flutter-driven TENG (CPF-TENG) with ambient air ionizing channel. Reprinted with permission from Ref. [119]. Copyright 2023, Wiley. (c) Lawn structured TENG based on the vertically free-standing polymer strips. Reprinted with permission from Ref. [120]. Copyright 2016, Wiley. (d) A flow-induced vibration effect based TENG. Reprinted with permission from Ref. [39]. Copyright 2021, Wiley. (e–h) TENG based on FT mode. (e) A multifunctional TENG for simultaneously harvesting water wave energy, water flow energy, and wind energy. Reprinted with permission from Ref. [7]. Copyright 2017, Wiley. (f) A rotary TENG using rabbit-fur-based soft-contact (SCR-TENG) with segmented structure. Reprinted with permission from Ref. [91]. Copyright 2022, Wiley. (g) A floating self-excited sliding TENG (FSS-TENG) by a self-excited amplification between rotator and stator to achieve self-increased charge density. Reprinted with permission from Ref. [42]. Copyright 2021, Springer Nature. (h) A self-excited liquid suspension TENG (LS-TENG) with optimized charge transportation behavior. Reprinted with permission from Ref. [126]. Copyright 2023, Wiley.

Table 1. Summary of typical FEC-TENGs.

Devices	Basic Output Performance									Energy Source	Stability	Encapsulation State	Networking
	Working Mode	Q_{SC} (μC)	I_{SC}	V_{OC} (V)	f_{min}	Effective Volume or Area	Matching Impedance	Peak Power Density	Average Power Density				
Hybrid nanogenerator [59]	CS	0.55	41.3 μA (1.25 Hz)	567	0.25 Hz	400 cm^2	60 $M\Omega$	0.5625 $W m^{-2} Hz^{-1}$	No	Water	100% (800 k)	Non-encapsulated	No
NPU-TENG [95]	LS	0.8	18 μA (1 Hz)	384	1 Hz	432 cm^3	5 $M\Omega$	1.97 $W m^{-3} Hz^{-1}$	No	Water	93.83% (45 k)	Non-encapsulated	Yes
B-TENG [99]	CS	1.45	75.35 μA (1.25 Hz)	707	1 Hz	1936 cm^3	15 $M\Omega$	No	7.65 $W m^{-3} Hz^{-1}$	Water	No	Encapsulated	No
HW-NG [58]	CS	No	28 μA (2 Hz)	580	0.5 Hz	41.95 cm^2	10 $M\Omega$	0.273 $W m^{-2} Hz^{-1}$	No	Water	100% (130 k)	Encapsulated	Yes
OB-TENG [100]	CS	26	450 μA (1.15 Hz)	650	0.2 Hz	4000 cm^3	13 $M\Omega$	9.675 $W m^{-3} Hz^{-1}$	0.863 $W m^{-3} Hz^{-1}$	Water	No	Encapsulated	No
BCHNG [101]	CS	2.2	700 μA (2 Hz)	900	1 $m s^{-2}$	400 cm^3	1 $M\Omega$	196 $W m^{-3}$	5.7 $W m^{-3}$	Water	80% (250 k)	Encapsulated	No
MH-TENG [102]	CS	2.9	200.3 μA (1 Hz)	268	0.6 Hz	690 cm^3	1 $M\Omega$	23.2 $W m^{-2} Hz^{-1}$	No	Water	97.1% (36 k)	Encapsulated	Yes
WF-TENG [103]	CS	1.2	85 μA (1.4 Hz)	450	0.8 Hz	519 cm^3	10 $M\Omega$	8.86 $W m^{-3} Hz^{-1}$	0.386 $W m^{-3} Hz^{-1}$	Water	No	Encapsulated	Yes
AR-TENG [37]	CS	0.7	122 μA (2 $m s^{-2}$)	66	1 $m s^{-2}$	2722 cm^3	5 $M\Omega$	4.59 $W m^{-3}$	No	Water	No	Encapsulated	No
IPM-TENG [36]	CS	0.6	15 μA (1 Hz)	150	0.5 Hz	268 cm^3	5 $M\Omega$	75 $W m^{-3} Hz^{-1}$	3.15 $W m^{-3} Hz^{-1}$	Water	No	Encapsulated	No
BBW-TENG [104]	FT	0.32	3.5 μA (1 Hz)	410	0.1 Hz	2144 cm^3	200 $M\Omega$	0.32 $W m^{-3} Hz^{-1}$	No	Water	100% (45 days)	Encapsulated	No
A hexagonal TENG [105]	CS	No	270 μA (1 Hz)	354	0.5 Hz	3660 cm^3	1.2 $M\Omega$	3.33 $W m^{-3} Hz^{-1}$	No	Water	No	Encapsulated	Yes
Spherical TENG [78]	CS	No	200 μA (1 Hz)	250	0.5 Hz	1767.2 cm^3	1 $M\Omega$	4.81 $W m^{-3} Hz^{-1}$	No	Water	No	Encapsulated	No
Spherical TENG with CEMs [35]	CS	No	15.1 mA (1.2 Hz)	16	0.7 Hz	4188.8 cm^3	680 $k\Omega$	4.93 $W m^{-3} Hz^{-1}$	0.05 $W m^{-3} Hz^{-1}$	Water	No	Encapsulated	No
TD-TENG [40]	FT	3.3	675 μA (0.58 Hz)	335	0.25 Hz	7500 cm^3	No	7.89 $W m^{-3} Hz^{-1}$	2.24 $W m^{-3} Hz^{-1}$	Water	No	Encapsulated	Yes
EC-TENG [80]	CS & FT	0.022	2 μA (1 Hz)	63	0.25 Hz	278.23 cm^3	48 $M\Omega$	0.323 $W m^{-3} Hz^{-1}$	No	Water	No	Encapsulated	Yes
EANG [43]	FT	0.086	27.7 μA (33.3 Hz)	270	1.67 Hz	56.55 cm^3	4 $M\Omega$	0.558 $W m^{-3} Hz^{-1}$	No	Water & wind	100% (50 k)	Encapsulated	No
WLM-TENG [110]	FT	1.1	20 μA (1 Hz)	3000	0.25 Hz	35.5 cm^2	200 $M\Omega$	14.1 $W m^{-3} Hz^{-1}$	0.842 $W m^{-3} Hz^{-1}$	Water	No	Non-encapsulated	No
T-TENG [111]	FT	0.24	8.5 μA (1.6 Hz)	~580	0.6 Hz	No	No	6.625 $W m^{-3} Hz^{-1}$	No	Water	No	Encapsulated	Yes
ES-TENG [44]	FT	0.027	0.74 μA	75.6	0.138 Hz	603.19 cm^3	100 $M\Omega$	0.046 $W m^{-3}$	No	Water & wind	97.24% (2000 k)	Encapsulated	Yes
GS-TENG [41]	FT	0.15	3.2 μA (6 $m s^{-2}$)	730	2 $m s^{-2}$	2140 cm^3	No	0.28 $W m^{-3}$	No	Water	92% (30 days)	Encapsulated	Yes
CEMA-TENG [112]	FT	0.796	47 μA (7 Hz)	240	1 Hz	127.55 cm^2	30 $M\Omega$	21.28 $W m^{-2}$	No	Water	94% (72 k)	Non-encapsulated	No
FIV-TENG [38]	CS	0.122	8.3 μA (7.8 $m s^{-1}$)	~292	2.9 $m s^{-1}$	72 cm^2	44 $M\Omega$	0.181 $W m_1^{-2}$ (7.8 $m s^{-1}$)	No	Wind	No	Non-encapsulated	Yes

Table 1. Cont.

Devices	Working Mode	Basic Output Performance								Energy Source	Stability	Encapsulation State	Networking
		Q_{SC} (μC)	I_{SC}	V_{OC} (V)	f_{min}	Effective Volume or Area	Matching Impedance	Peak Power Density	Average Power Density				
CAF-TENG [118]	CS	4700 (1 s)	36,000 μA (1.5 mL s ⁻¹)	508	1.5 mL s ⁻¹	25.1 cm ³	50 M Ω	No	26,000 W m ⁻³	Wind	No	Non-encapsulated	Yes
CPF-TENG [119]	CS	No	4.4 A (3.5 m s ⁻¹)	2560	2.8 m s ⁻¹	No	100 M Ω	No	425 W m ⁻²	Wind	100% (810 k)	Non-encapsulated	Yes
Lawn-structured TENG [120]	CS	No	12.5 μA (27 m s ⁻¹)	100	6 m s ⁻¹	No	10 M Ω	2.76 W m ⁻² (27 m s ⁻¹)	No	Wind	No	Non-encapsulated	Yes
F-TENG [39]	CS	0.09	10 μA (4.3 m s ⁻¹)	199	1.8 m s ⁻¹	No	50 M Ω	1.35 W m ⁻² (4.3 m s ⁻¹)	No	Wind	96% (100 k)	Non-encapsulated	Yes
Multifunctional TENG [7]	FT	0.275	21 μA (200 rpm)	490	10 rpm	44.18 cm ²	80 M Ω	No	0.034 W m ⁻² (2 Hz)	Water & wind	No	Non-encapsulated	No
SCR-TENG [91]	FT	0.342	20 μA (6 m s ⁻¹)	No	1 m s ⁻¹	No	300 M Ω	2.3 W m ⁻² (6 m s ⁻¹)	No	Wind	No	Non-encapsulated	Yes
FSS-TENG [42]	FT	0.4	17.6 μA (7 m s ⁻¹)	150	3 m s ⁻¹	23.3 cm ²	120 M Ω	7.16 W m ⁻² (7 m s ⁻¹)	No	Wind	100% (100 k)	Non-encapsulated	No
LS-TENG [126]	FT	0.871	106 μA (9 m s ⁻¹)	5400	1 m s ⁻¹	No	130 M Ω	23.9 W m ⁻² (8 m s ⁻¹)	4.4 W m ⁻² (8 m s ⁻¹)	Wind	100% (234 k)	Non-encapsulated	No

5. Summary and Applications of FEC-TENGs

Thanks to excellent output performance and a variety of structural designs, FEC-TENGs can be applied to a variety of scenarios. We divide them into four major fields: power supply, self-powered sensors, smart agriculture, and self-powered electrochemical systems, as shown in Figure 10.

Compared with electromagnetic generators, FEC-TENGs are better at collecting low-frequency mechanical energy. Therefore, as a portable energy supply source, FEC-TENGs often provide power for distributed electronic equipment networks [17,127,128]. For example, FSS-TENG converted a low wind speed of about 2 m s^{-1} into electrical energy to supply power for signage lights and thermometers [42]. Similarly, by collecting wind and water energy, the energy supply network integrated with ES-TENG can drive electronic products to form a self-powered environmental monitoring system [44]. By collecting water energy, HW-NG provided energy for long-distance wireless transmission equipment, forming a self-powered path avoidance warning system [58].

Since TENGs can directly convert mechanical stimuli into electrical signals, FEC-TENGs have great advantages as self-powered sensors for real-time transmission of relevant parameters in the natural environment [129–131]. LS-TENG can provide various real-time environmental information to the environmental sensor system by supplying power to various wireless sensors and signs [126]. An environmental monitoring network based on TENG was established, which can realize real-time, distributed, and wireless wide-area environmental monitoring [132]. By using several nodes, the sensor network covers an area of two square kilometers and shows great effectiveness and significance in long-term detection. Moreover, based on the active vibration sensor units with a spring-mass-based TENG, Wu et al. proposed an online monitoring vibration system, which provides a new idea for wind vibration monitoring of transmission lines using TENG technology [133].

Furthermore, due to the high voltage and low current output characteristics of TENGs, the high voltage applications based on FEC-TENGs focus on smart agriculture, which shows the safety and portability of this kind of TENG [31,123,134]. Based on the ternary dielectric triboelectrification effect [100], Li et al. designed a rotary TENG based on soft polyester fur, which can generate 15 kV DC voltage and 10 kV AC voltage [31]. In addition, based on the high-voltage output of the TENG, the author established a high-voltage processing device for processing plant seeds [31]. The experimental results showed that the tomato seed vigor index was greatly improved after treatment. Similarly, an all-weather TENG is used to drive various agricultural sensors and stimulate seeds, optimizing the growth environment of crops [135]. The self-powered system based on SCR-TENG can be applied to nighttime indication, insect trapping, soil moisture detection, environmental temperature and humidity detection, etc., showing the prospect of smart agriculture based on FEC-TENGs [93]. In addition, a large number of experimental applications based on FEC-TENGs have shown broad prospects in the field of smart agriculture [136,137].

As one of the most important research techniques, electrochemistry has been widely used in our lives. However, the demand for external power sources hinders the further development of electrochemistry. The electrochemical system based on TENG has always been a research hotspot [138]. In recent years, the self-powered electrochemical system based on FEC-TENGs has removed the shackles of external power sources and greatly promoted the sustainable development of electrochemical systems [48,139]. Han et al. used TENG to construct an electrocatalytic ammonia synthesis system with air as the nitrogen source, which can simultaneously perform nitrogen fixation and electrocatalytic reduction [140]. Based on the marine self-charging power supply system composed of seawater supercapacitors and FEC-TENG modules, Zhang et al. realized the DC output to drive electronics and sensors for ships in the marine environment, showing competitive potential in the field of intelligent oceans [141]. Moreover, Yang et al. made a hybrid nanogenerator to realize the acquisition of all-round, broadband low-frequency random micro-vibration energy [142]. Additionally, based on this hybrid nanogenerator, the author further developed a truly self-powered seawater diversion system and an electrochemical

cathodic protection system, which directly converts water energy into hydrogen energy to achieve self-corrosion of ships.

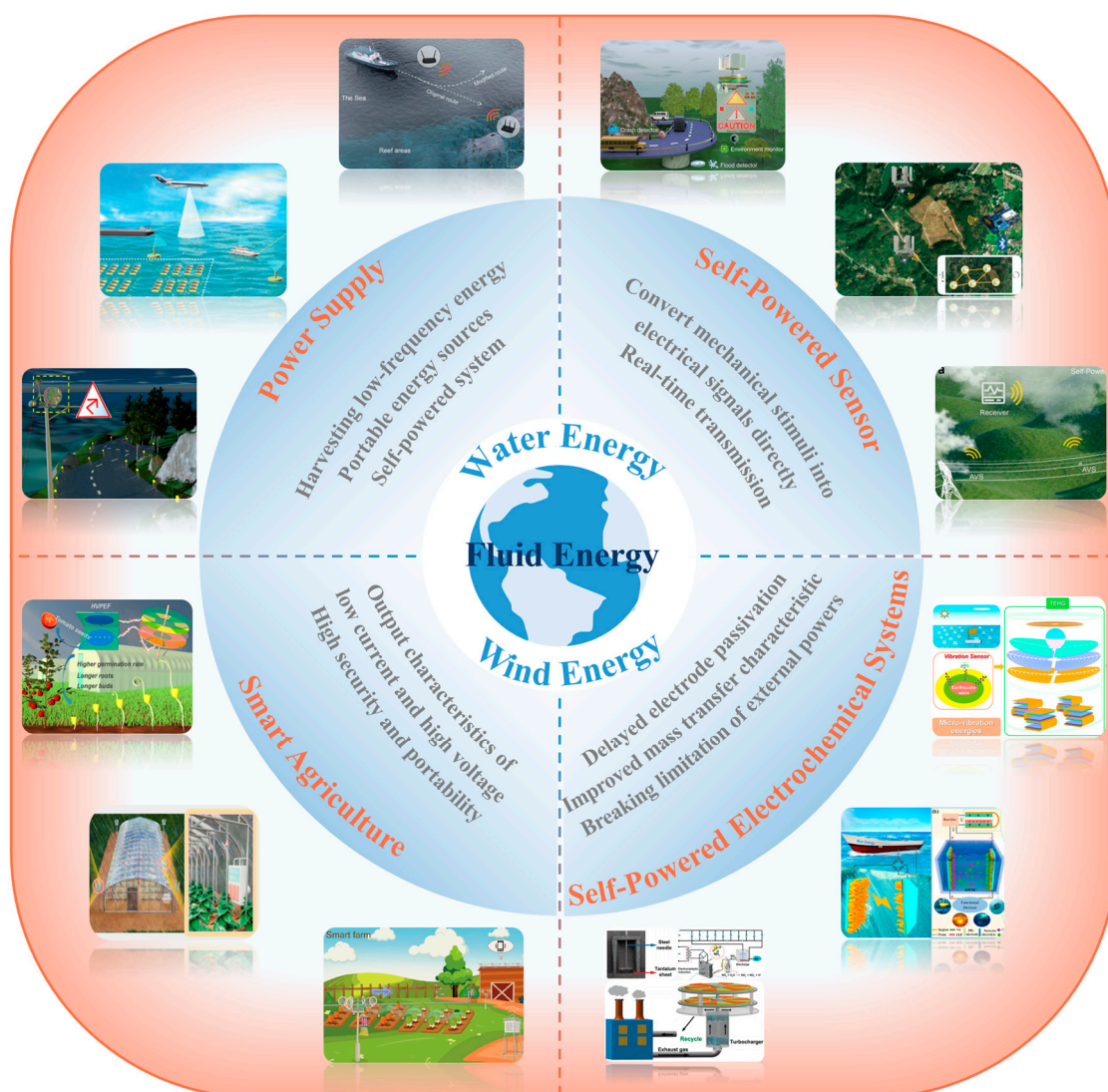


Figure 10. Summary and applications of TENG collecting fluid energy in power supply, self-powered sensors, smart agriculture, and self-powered electrochemical systems. Reprinted with permission from Ref. [42]. Copyright 2021, Springer Nature. Reprinted with permission from Ref. [44]. Copyright 2021, Wiley. Reprinted with permission from Ref. [58]. Copyright 2021, Wiley. Reprinted with permission from Ref. [126]. Copyright 2023, Wiley. Reprinted with permission from Ref. [132]. Copyright 2023, Wiley. Reprinted with permission from Ref. [133]. Copyright 2022, Wiley. Reprinted with permission from Ref. [31]. Copyright 2021, Elsevier. Reprinted with permission from Ref. [91]. Copyright 2022, Wiley. Reprinted with permission from Ref. [135]. Copyright 2022, Springer Nature. Reprinted with permission from Ref. [140]. Copyright 2020, Royal Society of Chemistry. Reprinted with permission from Ref. [141]. Copyright 2022, American Chemical Society. Reprinted with permission from Ref. [142]. Copyright 2020, American Chemical Society.

Furthermore, the self-powered electrochemical system based on FEC-TENGs has made a lot of contributions to pollutant treatment, electrochromic reaction, and so on [143–146]. Li et al. used the triboelectric effect to detect and remove heavy metal ions by self-energy [143]. The triboelectric nanosensors developed by them can selectively detect common heavy metal ions, such as Cu^{2+} , Pb^{2+} , and Cr^{3+} . They used a water-driven triboelectric nanogenerator (WD-TENG) to obtain kinetic energy from wastewater and could remove 97.4% of metal ions in

wastewater within 100 min [143]. Moreover, the use of the β -cyclodextrin pathway to enhance the triboelectric effect of self-powered phenol detection and electrochemical degradation was discovered [144]. The device obtains kinetic energy from the wastewater wave and electrochemically degrades phenol in a self-powered manner without using an external power supply, demonstrating another expanded application of FEC-TENGs [144]. By combining the electrochromic device (ECD) with the transparent TENG driven by wind and rain, Yeh et al. developed a self-powered smart window system [146]. This study reflects the substantial progress in the practical application of FEC-TENGs and self-powered systems.

Interestingly, a biomimetic stretchable nanogenerator for underwater energy harvesting was proposed by Zon et al. [147]. The nanogenerator mimics the structure of the ion channel on the cell membrane of the electric eel, which can obtain mechanical energy from underwater human motion and output an open circuit voltage of more than 10 V [147]. This study demonstrates that FEC-TENGs can provide sustainable energy for underwater soft wearable electronic devices. Based on an air-bag triboelectric nanogenerator (AS-TENG) coated with an antibacterial coating, Wang et al. developed a multifunctional fish-wearable data snooping platform (FDSP) for studying fish kinematics [148]. AS-TENG can not only obtain energy from the swimming of fish but also act as a self-powered sensory module to monitor the swimming behavior of fish [148]. This study demonstrates the broad application prospects of FEC-TENGs in underwater self-powered sensors, wearable tracking devices, soft robots, etc.

It can be seen that although the energy output of TENGs is lower than that of EMGs, the experimental results based on the above applications prove the safety, convenience, and expansibility of FEC-TENGs in the fields of energy supply, self-powered sensors, smart agriculture, and self-powered electrochemical systems.

6. Summary and Outlook

Through theoretical simulation and ingenious structural design, TENG converts irregular, random, and low-frequency fluid energy into electrical energy or electrical signals, which is required for sustainable energy in the new era. In this review, the working principle, working mode, structural design, and output performance of TENG for collecting fluid energy are systematically introduced. According to literature research, we find that most of the FEC-TENGs used CS and FT working modes. Moreover, starting from the energy conversion efficiency of FEC-TENGs, this review elaborates on the four processes of fluid energy conversion into available electric energy and illustrates the energy conversion efficiency in each energy conversion process. Subsequently, the remarkable achievements of FEC-TENGs in unidirectional energy collection and omnidirectional energy collection are reviewed from two aspects: water energy collection and wind energy collection. The detailed performance comparison of FEC-TENGs is shown in Table 1. Finally, we summarize the applications of FEC-TENGs in detail from four aspects: power supply, self-powered sensor, smart agriculture, and self-powered electrochemical system. Although significant progress and achievements have been made in the research and application of FEC-TENGs, to further develop the field, the following issues should be addressed to promote further development of this field:

- (1) Average Power Density Stability, and Reliability of FEC-TENGs. As the energy supply source, the average power density and stability of FEC-TENGs are particularly important. However, most studies only calculate the peak power density and ignore the stability of the devices, which hinders the further improvement of performance. We recommend that researchers standardize the calculation of the average power density and use the average power density as the basic output performance index of FEC-TENGs. Moreover, the stability of various devices should also be included in the scope of the investigation. The author should clarify what measures have been taken to improve the stability and reliability of the device, and test and record the stability and reliability of the device in the natural environment. The device's tolerance to humidity and temperature should also be systematically tested.

- (2) Energy Conversion Efficiency of FEC-TENGs. Although some studies have shown that detailed analysis of the energy conversion process and improving the energy conversion efficiency of FEC-TENGs can effectively improve output performance, most studies do not calculate the energy conversion efficiency. Therefore, we suggest that energy conversion efficiency should be included in the basic performance evaluation of FEC-TENGs, which is a necessary measure to further improve its output performance.
- (3) The Fabrication and Management Circuits of the FEC-TENGs. The device structure design should be simple and effective, with a certain theoretical support. A too-complex structure design not only reduces the energy conversion efficiency but also reduces the stability and reliability of FEC-TENGs to a certain extent. Moreover, the research on appropriate management circuits is still relatively lacking. FEC-TENGs have high-voltage and low-current output characteristics. When using FEC-TENGs to power a small electronic network, an appropriate energy management circuit is essential. Although some FEC-TENGs adopt energy management circuits that reduce voltage and increase current, there is still a lack of matching strategies between FEC-TENGs and related management circuits, which hinders the further application of FEC-TENGs. In addition, there is a lack of modular energy management circuits based on FEC-TENGs. In the face of a complex natural environment, non-periodic trigger conditions put forward higher requirements for management circuits.
- (4) Combination with Direct-Current TENGs (DC-TENGs). Thanks to the DC output, DC-TENGs are superior to AC-TENGs in terms of energy supply [98]. DC-TENGs can directly supply power to some electronic devices (without a rectifier), further simplifying the energy management circuit [130]. However, in the study based on FEC-TENGs, we rarely found the use of DC-TENGs to collect fluid energy. We believe that the steady DC output of DC-TENGs combined with the ubiquitous fluid energy will be an interesting story.
- (5) The Use of Environmentally Friendly and Degradable Materials in FEC-TENGs. Considering that the application scenarios of FEC-TENGs are mostly rivers, lakes, and field environments, we strongly recommend that researchers use environmentally friendly and degradable triboelectric materials and packaging materials to manufacture FEC-TENGs. Environmentally friendly degradable materials can be plant leaves and animal fur. Some excellent triboelectric materials with animals and plants as degradable raw materials will not lead to the gradual degradation of device performance. Moreover, for other environmentally friendly materials, we recommend some degradable materials that can be controlled for degradation for FEC-TENGs. For example, degradation materials such as alginate and rice paper can achieve preliminary controllable degradation [74].
- (6) The Commercial Development of FEC-TENGs. Studies have shown that FEC-TENGs can improve the overall energy collection efficiency through a networked mode. However, to commercialize FEC-TENGs, it is far from enough to improve the output performance. Programmable manufacturing, intelligent network connection, unified energy management, and subsequent management of equipment are all urgent problems to be solved in the commercialization process of FEC-TENGs.
- (7) Challenges of the Future Applications of FEC-TENGs. Although the application of FEC-TENGs has spread across many fields, we should apply FEC-TENG technology to more fields, such as self-powered underwater detection equipment and high-altitude wind energy collectors. Furthermore, the application environment of FEC-TENGs is mostly the natural environment. For devices used in smart agriculture and self-powered systems, it is necessary to use appropriate back-end devices for energy storage and signal transmission. For harsh outdoor environments, FEC-TENGs must have stronger moisture resistance, heat resistance, sun protection, and corrosion resistance.

Author Contributions: Conceptualization, Q.L. and Y.X.; writing—original draft preparation, Q.L.; writing—review and editing, Q.L. and Y.X.; supervision, Y.X.; project administration, Q.L. and Y.X.; funding acquisition, Y.X. All authors have read and agreed to the published version of the manuscript.

Funding: This research was funded by the National Natural Science Foundation of China (NSFC) (52272191, U21A20147, 52073037, 52202212), National Key R & D Project from Minister of Science and Technology (2021YFA1201602), and National Natural Science Foundation of Chongqing (cstc2019cyj-msxmX0068, SCTB2022NSCQ-MSX0942).

Data Availability Statement: No new data were created or analyzed in this study. Data sharing is not applicable to this article.

Conflicts of Interest: The authors declare no conflict of interest.

References

1. Xiao, Q.; Zhu, Q. A review on flow energy harvesters based on flapping foils. *J. Fluid. Struct.* **2014**, *46*, 174–191. [[CrossRef](#)]
2. Stevens, R.J.A.M.; Meneveau, C. Flow structure and turbulence in wind farms. *Annu. Rev. Fluid Mech.* **2017**, *49*, 311–339. [[CrossRef](#)]
3. Wang, Z.; Wang, Y.; Gao, Q.; Bao, G.; Cheng, T.; Wang, Z.L. Triboelectric fluid sensors: Principles, development, and perspectives. *Adv. Mater. Technol.* **2023**, *8*, 2201029. [[CrossRef](#)]
4. Wang, Z.L.; Jiang, T.; Xu, L. Toward the blue energy dream by triboelectric nanogenerator networks. *Nano Energy* **2017**, *39*, 9–23. [[CrossRef](#)]
5. Wang, Z.L. Triboelectric nanogenerator (TENG)-sparking an energy and sensor revolution. *Adv. Energy Mater.* **2020**, *10*, 2000137. [[CrossRef](#)]
6. Hu, J.; Pu, X.; Yang, H.; Zeng, Q.; Tang, Q.; Zhang, D.; Hu, C.; Xi, Y. A flutter-effect-based triboelectric nanogenerator for breeze energy collection from arbitrary directions and self-powered wind speed sensor. *Nano Res.* **2019**, *12*, 3018–3023. [[CrossRef](#)]
7. Xi, Y.; Guo, H.; Zi, Y.; Li, X.; Wang, J.; Deng, J.; Li, S.; Hu, C.; Cao, X.; Wang, Z.L. Multifunctional TENG for blue energy scavenging and self-powered wind-speed sensor. *Adv. Energy Mater.* **2017**, *7*, 1602397. [[CrossRef](#)]
8. Siria, A.; Bocquet, M.-L.; Bocquet, L. New avenues for the large-scale harvesting of blue energy. *Nat. Rev. Chem.* **2017**, *1*, 91. [[CrossRef](#)]
9. Jiang, T.; Zhang, L.M.; Chen, X.; Han, C.B.; Tang, W.; Zhang, C.; Xu, L.; Wang, Z.L. Structural optimization of triboelectric nanogenerator for harvesting water wave energy. *ACS Nano* **2015**, *9*, 12562–12572. [[CrossRef](#)] [[PubMed](#)]
10. Choi, D.; Lee, Y.; Lin, Z.-H.; Cho, S.; Kim, M.; Ao, C.K.; Soh, S.; Sohn, C.; Jeong, C.K.; Lee, J.; et al. Recent advances in triboelectric nanogenerators: From technological progress to commercial applications. *ACS Nano* **2023**, *17*, 11087–11219. [[CrossRef](#)]
11. Kim, W.-G.; Kim, D.-W.; Tcho, I.-W.; Kim, J.-K.; Kim, M.-S.; Choi, Y.-K. Triboelectric nanogenerator: Structure, mechanism, and applications. *ACS Nano* **2021**, *15*, 258–287. [[CrossRef](#)] [[PubMed](#)]
12. Liu, R.; Wang, Z.L.; Fukuda, K.; Someya, T. Flexible self-charging power sources. *Nat. Rev. Mater.* **2022**, *7*, 870–886. [[CrossRef](#)]
13. Mariello, M.; Guido, F.; Mastronardi, V.M.; Todaro, M.T.; Desmaele, D.; De Vittorio, M. Nanogenerators for harvesting mechanical energy conveyed by liquids. *Nano Energy* **2019**, *57*, 141–156. [[CrossRef](#)]
14. Zi, Y.; Guo, H.; Wen, Z.; Yeh, M.-H.; Hu, C.; Wang, Z.L. Harvesting low-frequency (<5 Hz) irregular mechanical energy: A possible killer application of triboelectric nanogenerator. *ACS Nano* **2016**, *10*, 4797–4805. [[CrossRef](#)] [[PubMed](#)]
15. Lee, J.-H.; Lee, K.Y.; Kumar, B.; Nguyen Thanh, T.; Lee, N.-E.; Kim, S.-W. Highly sensitive stretchable transparent piezoelectric nanogenerators. *Energy Environ. Sci.* **2013**, *6*, 169–175. [[CrossRef](#)]
16. Wang, Z.L. On the First principle theory of nanogenerators from maxwell's equations. *Nano Energy* **2020**, *68*, 104272. [[CrossRef](#)]
17. Luo, J.; Wang, Z.L. Recent progress of triboelectric nanogenerators: From fundamental theory to practical applications. *EcoMat* **2020**, *2*, e12059. [[CrossRef](#)]
18. Cheng, T.; Gao, Q.; Wang, Z.L. The current development and future outlook of triboelectric nanogenerators: A survey of literature. *Adv. Mater. Technol.* **2019**, *4*, 1800588. [[CrossRef](#)]
19. Shan, C.; Liu, W.; Wang, Z.; Pu, X.; He, W.; Tang, Q.; Fu, S.; Li, G.; Long, L.; Guo, H.; et al. An inverting TENG to realize the AC mode based on the coupling of triboelectrification and air-breakdown. *Energy Environ. Sci.* **2021**, *14*, 5395–5405. [[CrossRef](#)]
20. He, W.; Shan, C.; Wu, H.; Fu, S.; Li, Q.; Li, G.; Zhang, X.; Du, Y.; Wang, J.; Wang, X.; et al. Capturing dissipation charge in charge space accumulation area for enhancing output performance of sliding triboelectric nanogenerator. *Adv. Energy Mater.* **2022**, *12*, 2201454. [[CrossRef](#)]
21. Liu, D.; Zhou, L.; Wang, Z.L.; Wang, J. Triboelectric nanogenerator: From alternating current to direct current. *Iscience* **2021**, *24*, 102018. [[CrossRef](#)] [[PubMed](#)]
22. Shan, C.; He, W.; Wu, H.; Fu, S.; Tang, Q.; Wang, Z.; Du, Y.; Wang, J.; Guo, H.; Hu, C. A high-performance bidirectional direct current TENG by triboelectrification of two dielectrics and local corona discharge. *Adv. Energy Mater.* **2022**, *12*, 2200963. [[CrossRef](#)]
23. Shan, C.; Li, K.; Cheng, Y.; Hu, C. Harvesting environment mechanical energy by direct current triboelectric nanogenerators. *Nano-Micro Lett.* **2023**, *15*, 127. [[CrossRef](#)]

24. Hinchet, R.; Yoon, H.-J.; Ryu, H.; Kim, M.-K.; Choi, E.-K.; Kim, D.-S.; Kim, S.-W. Transcutaneous ultrasound energy harvesting using capacitive triboelectric technology. *Science* **2019**, *365*, 491–494. [[CrossRef](#)] [[PubMed](#)]
25. Lee, Y.-S.; Jeon, S.; Kim, D.; Lee, D.-M.; Kim, D.; Kim, S.-W. High performance direct current-generating triboelectric nanogenerators based on tribovoltaic p-n junction with ChCl-passivated CsFAMA perovskite. *Nano Energy* **2023**, *106*, 108066. [[CrossRef](#)]
26. Fan, F.R.; Tian, Z.Q.; Wang, Z.L. Flexible triboelectric generator! *Nano Energy* **2012**, *1*, 328–334. [[CrossRef](#)]
27. Xia, X.; Zhou, Z.; Shang, Y.; Yang, Y.; Zi, Y. Metallic glass-based triboelectric nanogenerators. *Nat. Commun.* **2023**, *14*, 1023. [[CrossRef](#)]
28. Li, Q.; Fu, S.; Li, X.; Chen, H.; He, W.; Yang, Q.; Zhang, X.; Yang, H.; Ren, D.; Xi, Y. Overall performance improvement of direct-current triboelectric nanogenerators by charge leakage and ternary dielectric evaluation. *Energy Environ. Sci.* **2023**, *16*, 3414–3525. [[CrossRef](#)]
29. Zou, H.; Zhang, Y.; Guo, L.; Wang, P.; He, X.; Dai, G.; Zheng, H.; Chen, C.; Wang, A.C.; Xu, C.; et al. Quantifying the triboelectric series. *Nat. Commun.* **2019**, *10*, 1427. [[CrossRef](#)]
30. Yang, H.; Lai, J.a.; Li, Q.; Zhang, X.; Li, X.; Yang, Q.; Hu, Y.; Xi, Y.; Wang, Z.L. High-sensitive and ultra-wide spectrum multifunctional triboelectric acoustic sensor for broad scenario applications. *Nano Energy* **2022**, *104*, 107932. [[CrossRef](#)]
31. Li, Q.; Liu, W.; Yang, H.; He, W.; Long, L.; Wu, M.; Zhang, X.; Xi, Y.; Hu, C.; Wang, Z.L. Ultra-stability high-voltage triboelectric nanogenerator designed by ternary dielectric triboelectrification with partial soft-contact and non-contact mode. *Nano Energy* **2021**, *90*, 106585. [[CrossRef](#)]
32. Zhang, X.; Yang, Q.; Ren, D.; Yang, H.; Li, X.; Li, Q.; Liu, H.; Hu, C.; He, X.; Xi, Y. Omnidirectional water wave-driven triboelectric net-zero power smart ocean network: An advanced hardware solution to long-distance target detection. *Nano Energy* **2023**, *114*, 108614. [[CrossRef](#)]
33. Fu, S.; Wu, H.; He, W.; Li, Q.; Shan, C.; Wang, J.; Du, Y.; Du, S.; Huang, Z.; Hu, C. Conversion of dielectric surface effect into volume effect for high output energy. *Adv. Mater.* **2023**, *35*, 2302954. [[CrossRef](#)]
34. Tian, J.; Chen, X.; Wang, Z.L. Environmental energy harvesting based on triboelectric nanogenerators. *Nanotechnology* **2020**, *31*, 242001. [[CrossRef](#)]
35. Liang, X.; Liu, S.; Ren, Z.; Jiang, T.; Wang, Z.L. Self-powered intelligent buoy based on triboelectric nanogenerator for water level alarming. *Adv. Funct. Mater.* **2022**, *32*, 2205313. [[CrossRef](#)]
36. Zhang, X.; Yang, Q.; Ji, P.; Wu, Z.; Li, Q.; Yang, H.; Li, X.; Zheng, G.; Xi, Y.; Wang, Z.L. Modeling of liquid-solid hydrodynamic water wave energy harvesting system based on triboelectric nanogenerator. *Nano Energy* **2022**, *99*, 107362. [[CrossRef](#)]
37. Zhang, C.G.; He, L.X.; Zhou, L.L.; Yang, O.; Yuan, W.; Wei, X.L.; Liu, Y.B.; Lu, L.; Wang, J.; Wang, Z.L. Active resonance triboelectric nanogenerator for harvesting omnidirectional water-wave energy. *Joule* **2021**, *5*, 1613–1623. [[CrossRef](#)]
38. Zeng, Q.; Wu, Y.; Tang, Q.; Liu, W.; Wu, J.; Zhang, Y.; Yin, G.; Yang, H.; Yuan, S.; Tan, D.; et al. A high-efficient breeze energy harvester utilizing a full-packaged triboelectric nanogenerator based on flow-induced vibration. *Nano Energy* **2020**, *70*, 104524. [[CrossRef](#)]
39. Zhang, X.; Hu, J.; Yang, Q.; Yang, H.; Yang, H.; Li, Q.; Li, X.; Hu, C.; Xi, Y.; Wang, Z.L. Harvesting multidirectional breeze energy and self-powered intelligent fire detection systems based on triboelectric nanogenerator and fluid-dynamic modeling. *Adv. Funct. Mater.* **2021**, *31*, 2106527. [[CrossRef](#)]
40. Bai, Y.; Xu, L.; He, C.; Zhu, L.; Yang, X.; Jiang, T.; Nie, J.; Zhong, W.; Wang, Z.L. High-performance triboelectric nanogenerators for self-powered, in situ and real-time water quality mapping. *Nano Energy* **2019**, *66*, 104117. [[CrossRef](#)]
41. Gao, Q.; Xu, Y.; Yu, X.; Jing, Z.; Cheng, T.; Wang, Z.L. Gyroscope-structured triboelectric nanogenerator for harvesting multidirectional ocean wave energy. *ACS Nano* **2022**, *16*, 6781–6788. [[CrossRef](#)]
42. Long, L.; Liu, W.; Wang, Z.; He, W.; Li, G.; Tang, Q.; Guo, H.; Pu, X.; Liu, Y.; Hu, C. High performance floating self-excited sliding triboelectric nanogenerator for micro mechanical energy harvesting. *Nat. Commun.* **2021**, *12*, 4689. [[CrossRef](#)] [[PubMed](#)]
43. Zhong, Y.; Zhao, H.; Guo, Y.; Rui, P.; Shi, S.; Zhang, W.; Liao, Y.; Wang, P.; Wang, Z.L. An easily assembled electromagnetic-triboelectric hybrid nanogenerator driven by magnetic coupling for fluid energy harvesting and self-powered flow monitoring in a smart home/city. *Adv. Mater. Technol.* **2019**, *4*, 1900741. [[CrossRef](#)]
44. Lin, Z.; Zhang, B.; Xie, Y.; Wu, Z.; Yang, J.; Wang, Z.L. Elastic-connection and soft-contact triboelectric nanogenerator with superior durability and efficiency. *Adv. Funct. Mater.* **2021**, *31*, 2105237. [[CrossRef](#)]
45. Yuan, S.; Zeng, Q.; Tan, D.; Luo, Y.; Zhang, X.; Guo, H.; Wang, X.; Wang, Z.L. Scavenging breeze wind energy ($1\text{--}8.1\text{ m s}^{-1}$) by minimalist triboelectric nanogenerator based on the wake galloping phenomenon. *Nano Energy* **2022**, *100*, 107465. [[CrossRef](#)]
46. Wu, C.S.; Wang, A.C.; Ding, W.B.; Guo, H.Y.; Wang, Z.L. Triboelectric nanogenerator: A foundation of the energy for the new era. *Adv. Energy Mater.* **2019**, *9*, 1802906. [[CrossRef](#)]
47. Chen, B.; Wang, Z.L. Toward a new era of sustainable energy: Advanced triboelectric nanogenerator for harvesting high entropy energy. *Small* **2022**, *18*, 2107034. [[CrossRef](#)] [[PubMed](#)]
48. Zhou, L.L.; Liu, D.; Liu, L.; He, L.X.; Cao, X.; Wang, J.; Wang, Z.L. Recent advances in self-powered electrochemical systems. *Research* **2021**, *2021*, 4673028. [[CrossRef](#)]
49. Zhang, Q.; Xin, C.F.; Shen, F.; Gong, Y.; Zi, Y.L.; Guo, H.Y.; Li, Z.J.; Peng, Y.; Zhang, Q.; Wang, Z.L. Human body IoT systems based on the triboelectrification effect: Energy harvesting, sensing, interfacing and communication. *Energy Environ. Sci.* **2022**, *15*, 3688–3721. [[CrossRef](#)]

50. Chandrasekaran, S.; Bowen, C.; Roscow, J.; Zhang, Y.; Dang, D.K.; Kim, E.J.; Misra, R.D.K.; Deng, L.B.; Chung, J.S.; Hur, S.H. Micro-scale to nano-scale generators for energy harvesting: Self powered piezoelectric, triboelectric and hybrid devices. *Phys. Rep.* **2019**, *792*, 1–33. [[CrossRef](#)]
51. Zou, H.Y.; Guo, L.T.; Xue, H.; Zhang, Y.; Shen, X.F.; Liu, X.T.; Wang, P.H.; He, X.; Dai, G.Z.; Jiang, P.; et al. Quantifying and understanding the triboelectric series of inorganic non-metallic materials. *Nat. Commun.* **2020**, *11*, 2093. [[CrossRef](#)]
52. Liu, W.L.; Wang, Z.; Hu, C.G. Advanced designs for output improvement of triboelectric nanogenerator system. *Mater. Today* **2021**, *45*, 93–119. [[CrossRef](#)]
53. Chen, A.H.; Zhang, C.; Zhu, G.; Wang, Z.L. Polymer materials for high-performance triboelectric nanogenerators. *Adv. Sci.* **2020**, *7*, 2000186. [[CrossRef](#)]
54. Cui, X.; Yu, C.; Wang, Z.; Wan, D.; Zhang, H. Triboelectric nanogenerators for harvesting diverse water kinetic energy. *Micromachines* **2022**, *13*, 1219. [[CrossRef](#)]
55. Wu, X.; Li, X.; Ping, J.; Ying, Y. Recent advances in water-driven triboelectric nanogenerators based on hydrophobic interfaces. *Nano Energy* **2021**, *90*, 106592. [[CrossRef](#)]
56. Ren, Z.; Wu, L.; Pang, Y.; Zhang, W.; Yang, R. Strategies for effectively harvesting wind energy based on triboelectric nanogenerators. *Nano Energy* **2022**, *100*, 107522. [[CrossRef](#)]
57. Mariello, M.; Fachechi, L.; Guido, F.; De Vittorio, M. Multifunctional sub-100 μm thickness flexible piezo/triboelectric hybrid water energy harvester based on biocompatible AlN and soft parylene C-PDMS-EcoflexTM. *Nano Energy* **2021**, *83*, 105811. [[CrossRef](#)]
58. Ren, Z.; Liang, X.; Liu, D.; Li, X.; Ping, J.; Wang, Z.; Wang, Z.L. Water-wave driven route avoidance warning system for wireless ocean navigation. *Adv. Energy Mater.* **2021**, *11*, 2101116. [[CrossRef](#)]
59. Yang, H.; Deng, M.; Tang, Q.; He, W.; Hu, C.; Xi, Y.; Liu, R.; Wang, Z.L. A nonencapsulative pendulum-like paper-based hybrid nanogenerator for energy harvesting. *Adv. Energy Mater.* **2019**, *9*, 1901149. [[CrossRef](#)]
60. Zeng, Q.; Luo, Y.; Zhang, X.; Tan, L.; Chen, A.; Tang, Q.; Yang, H.; Wang, X. A bistable triboelectric nanogenerator for low-grade thermal energy harvesting and solar thermal energy conversion. *Small* **2023**, *19*, 2301952. [[CrossRef](#)]
61. Lai, Y.-C.; Hsiao, Y.-C.; Wu, H.-M.; Wang, Z.L. Waterproof fabric-based multifunctional triboelectric nanogenerator for universally harvesting energy from raindrops, wind, and human motions and as self-powered sensors. *Adv. Sci.* **2019**, *6*, 1801883. [[CrossRef](#)]
62. Xu, W.; Zheng, H.; Liu, Y.; Zhou, X.; Zhang, C.; Song, Y.; Deng, X.; Leung, M.; Yang, Z.; Xu, R.X.; et al. A droplet-based electricity generator with high instantaneous power density. *Nature* **2020**, *578*, 392–396. [[CrossRef](#)] [[PubMed](#)]
63. Hasan, M.A.M.; Zhang, T.; Wu, H.; Yang, Y. Water droplet-based nanogenerators. *Adv. Energy Mater.* **2022**, *12*, 2201383. [[CrossRef](#)]
64. Ye, C.; Liu, D.; Chen, P.; Cao, L.N.Y.; Li, X.; Jiang, T.; Wang, Z.L. An integrated solar panel with a triboelectric nanogenerator array for synergistic harvesting of raindrop and solar energy. *Adv. Mater.* **2023**, *35*, 2209713. [[CrossRef](#)]
65. Li, Z.; Yang, D.; Zhang, Z.; Lin, S.; Cao, B.; Wang, L.; Wang, Z.L.; Yin, F. A droplet-based electricity generator for large-scale raindrop energy harvesting. *Nano Energy* **2022**, *100*, 107443. [[CrossRef](#)]
66. Dong, J.; Zhu, L.; Guo, P.; Xu, C.; Zhao, X.; Yang, S.; He, X.; Zhou, G.; Ma, G.; Guo, H.; et al. A bio-inspired total current nanogenerator. *Energy Environ. Sci.* **2023**, *16*, 1071–1081. [[CrossRef](#)]
67. Dong, J.; Fan, F.R.; Tian, Z.-Q. Droplet-based nanogenerators for energy harvesting and self-powered sensing. *Nanoscale* **2021**, *13*, 17290–17309. [[CrossRef](#)]
68. Cheedarala, R.K.; Shahriar, M.; Ahn, J.H.; Hwang, J.Y.; Ahn, K.K. Harvesting liquid stream energy from unsteady peristaltic flow induced pulsatile Flow-TENG (PF-TENG) using slipping polymeric surface inside elastomeric tubing. *Nano Energy* **2019**, *65*, 104017. [[CrossRef](#)]
69. Jiang, P.; Zhang, L.; Guo, H.; Chen, C.; Wu, C.; Zhang, S.; Wang, Z.L. Signal output of triboelectric nanogenerator at oil-water-solid multiphase interfaces and its application for dual-signal chemical sensing. *Adv. Mater.* **2019**, *31*, 1902793. [[CrossRef](#)]
70. Chen, B.D.; Tang, W.; He, C.; Deng, C.R.; Yang, L.J.; Zhu, L.P.; Chen, J.; Shao, J.J.; Liu, L.; Wang, Z.L. Water wave energy harvesting and self-powered liquid-surface fluctuation sensing based on bionic-jellyfish triboelectric nanogenerator. *Mater. Today* **2018**, *21*, 88–97. [[CrossRef](#)]
71. Yoo, D.; Park, S.-C.; Lee, S.; Sim, J.-Y.; Song, I.; Choi, D.; Lim, H.; Kim, D.S. Biomimetic anti-reflective triboelectric nanogenerator for concurrent harvesting of solar and raindrop energies. *Nano Energy* **2019**, *57*, 424–431. [[CrossRef](#)]
72. Kwak, S.S.; Kim, S.M.; Ryu, H.; Kim, J.; Khan, U.; Yoon, H.-J.; Jeong, Y.H.; Kim, S.-W. Butylated melamine formaldehyde as a durable and highly positive friction layer for stable, high output triboelectric nanogenerators. *Energy Environ. Sci.* **2019**, *12*, 3156–3163. [[CrossRef](#)]
73. Kim, J.; Kang, D.; Lee, H.-K.; Hwang, J.-H.; Lee, H.Y.; Jeon, S.; Kim, D.; Kim, S.; Kim, S.-W. Design Principles to Maximize Non-Bonding States for Highly Tribopositive Behavior. *Adv. Funct. Mater.* **2023**, *33*, 2209648. [[CrossRef](#)]
74. Chao, S.; Ouyang, H.; Jiang, D.; Fan, Y.; Li, Z. Triboelectric nanogenerator based on degradable materials. *EcoMat* **2021**, *3*, e12072. [[CrossRef](#)]
75. Feng, Y.; Zhang, L.; Zheng, Y.; Wang, D.; Zhou, F.; Liu, W. Leaves based triboelectric nanogenerator (TENG) and TENG tree for wind energy harvesting. *Nano Energy* **2019**, *55*, 260–268. [[CrossRef](#)]
76. Choi, D.; Kim, D.W.; Yoo, D.; Cha, K.J.; La, M.; Kim, D.S. Spontaneous occurrence of liquid-solid contact electrification in nature: Toward a robust triboelectric nanogenerator inspired by the natural lotus leaf. *Nano Energy* **2017**, *36*, 250–259. [[CrossRef](#)]

77. Deng, Z.C.; Xu, L.; Qin, H.F.; Li, X.Y.; Duan, J.Z.; Hou, B.R.; Wang, Z.L. Rationally structured triboelectric nanogenerator arrays for harvesting water-current energy and self-powered sensing. *Adv. Mater.* **2022**, *34*, 2205064. [[CrossRef](#)]
78. Liang, X.; Jiang, T.; Liu, G.; Feng, Y.; Zhang, C.; Wang, Z.L. Spherical triboelectric nanogenerator integrated with power management module for harvesting multidirectional water wave energy. *Energy Environ. Sci.* **2020**, *13*, 277–285. [[CrossRef](#)]
79. He, W.; Liu, W.; Chen, J.; Wang, Z.; Liu, Y.; Pu, X.; Yang, H.; Tang, Q.; Yang, H.; Guo, H.; et al. Boosting output performance of sliding mode triboelectric nanogenerator by charge space-accumulation effect. *Nat. Commun.* **2020**, *11*, 4277. [[CrossRef](#)]
80. Tan, D.; Zeng, Q.; Wang, X.; Yuan, S.; Luo, Y.; Zhang, X.; Tan, L.; Hu, C.; Liu, G. Anti-overturning fully symmetrical triboelectric nanogenerator based on an elliptic cylindrical structure for all-weather blue energy harvesting. *Nano-Micro Lett.* **2022**, *14*, 124. [[CrossRef](#)]
81. Xu, Y.; Yang, W.; Lu, X.; Yang, Y.; Li, J.; Wen, J.; Cheng, T.; Wang, Z.L. Triboelectric nanogenerator for ocean wave graded energy harvesting and condition monitoring. *ACS Nano* **2021**, *15*, 16368–16375. [[CrossRef](#)] [[PubMed](#)]
82. Pang, H.; Feng, Y.; An, J.; Chen, P.; Han, J.; Jiang, T.; Wang, Z.L. Segmented swing-structured fur-based triboelectric nanogenerator for harvesting blue energy toward marine environmental applications. *Adv. Funct. Mater.* **2021**, *31*, 2106398. [[CrossRef](#)]
83. Lin, Z.; Zhang, B.; Guo, H.; Wu, Z.; Zou, H.; Yang, J.; Wang, Z.L. Super-robust and frequency-multiplied triboelectric nanogenerator for efficient harvesting water and wind energy. *Nano Energy* **2019**, *64*, 103908. [[CrossRef](#)]
84. Zhu, M.; Zhang, J.; Wang, Z.; Yu, X.; Zhang, Y.; Zhu, J.; Wang, Z.L.; Cheng, T. Double-blade structured triboelectric-electromagnetic hybrid generator with aerodynamic enhancement for breeze energy harvesting. *Appl. Energy* **2022**, *326*, 119970. [[CrossRef](#)]
85. Gao, X.; Xing, F.; Guo, F.; Yang, Y.; Hao, Y.; Chen, J.; Chen, B.; Wang, Z.L. A turbine disk-type triboelectric nanogenerator for wind energy harvesting and self-powered wildfire pre-warning. *Mater. Today Energy* **2021**, *22*, 100867. [[CrossRef](#)]
86. Tang, Q.; Pu, X.; Zeng, Q.; Yang, H.; Li, J.; Wu, Y.; Guo, H.; Huang, Z.; Hu, C. A strategy to promote efficiency and durability for sliding energy harvesting by designing alternating magnetic stripe arrays in triboelectric nanogenerator. *Nano Energy* **2019**, *66*, 104087. [[CrossRef](#)]
87. Yang, H.; Yang, H.; Lai, M.; Xi, Y.; Guan, Y.; Liu, W.; Zeng, Q.; Lu, J.; Hu, C.; Wang, Z.L. Triboelectric and electromagnetic hybrid nanogenerator based on a crankshaft piston system as a multifunctional energy harvesting device. *Adv. Mater. Technol.* **2019**, *4*, 1800278. [[CrossRef](#)]
88. Zhang, Y.; Zeng, Q.; Wu, Y.; Wu, J.; Yuan, S.; Tan, D.; Hu, C.; Wang, X. An ultra-durable windmill-like hybrid nanogenerator for steady and efficient harvesting of low-speed wind energy. *Nano-Micro Lett.* **2020**, *12*, 175. [[CrossRef](#)]
89. Han, K.; Luo, J.; Feng, Y.; Lai, Q.; Bai, Y.; Tang, W.; Wang, Z.L. Wind-driven radial-engine-shaped triboelectric nanogenerators for self-powered absorption and degradation of NO_x. *ACS Nano* **2020**, *14*, 2751–2759. [[CrossRef](#)]
90. Zhang, C.; Liu, Y.; Zhang, B.; Yang, O.; Yuan, W.; He, L.; Wei, X.; Wang, J.; Wang, Z.L. Harvesting wind energy by a triboelectric nanogenerator for an intelligent high-speed train system. *ACS Energy Lett.* **2021**, *6*, 1490–1499. [[CrossRef](#)]
91. Han, J.; Feng, Y.; Chen, P.; Liang, X.; Pang, H.; Jiang, T.; Wang, Z.L. Wind-driven soft-contact rotary triboelectric nanogenerator based on rabbit fur with high performance and durability for smart farming. *Adv. Funct. Mater.* **2022**, *32*, 2108580. [[CrossRef](#)]
92. Su, E.; Li, H.; Zhang, J.; Xu, Z.; Chen, B.; Cao, L.N.Y.; Wang, Z.L. Rationally designed anti-glare panel arrays as highway wind energy harvester. *Adv. Funct. Mater.* **2023**, *33*, 2214934. [[CrossRef](#)]
93. Hu, Y.; Li, Q.; Long, L.; Yang, Q.; Fu, S.; Liu, W.; Zhang, X.; Yang, H.; Hu, C.; Xi, Y. Matching mechanism of charge excitation circuit for boosting performance of a rotary triboelectric nanogenerator. *ACS Appl. Mater. Interfaces* **2022**, *14*, 48636–48646. [[CrossRef](#)]
94. Fu, X.; Xu, S.; Gao, Y.; Zhang, X.; Liu, G.; Zhou, H.; Lv, Y.; Zhang, C.; Wang, Z.L. Breeze-wind-energy-powered autonomous wireless anemometer based on rolling contact-electrification. *ACS Energy Lett.* **2021**, *6*, 2343–2350. [[CrossRef](#)]
95. Zhang, X.; Hu, J.; Zeng, Q.; Yang, H.; He, W.; Li, Q.; Li, X.; Yang, H.; Hu, C.; Xi, Y. A non-encapsulated polymorphous U-shaped triboelectric nanogenerator for multiform hydropower harvesting. *Adv. Mater. Technol.* **2021**, *6*, 2001199. [[CrossRef](#)]
96. Zhang, C.; Liu, L.; Zhou, L.; Yin, X.; Wei, X.; Hu, Y.; Liu, Y.; Chen, S.; Wang, J.; Wang, Z.L. Self-powered sensor for quantifying ocean surface water waves based on triboelectric nanogenerator. *ACS Nano* **2020**, *14*, 7092–7100. [[CrossRef](#)]
97. Xu, S.; Liu, G.; Wang, J.; Wen, H.; Cao, S.; Yao, H.; Wan, L.; Wang, Z.L. Interaction between water wave and geometrical structures of floating triboelectric nanogenerators. *Adv. Energy Mater.* **2022**, *12*, 2103408. [[CrossRef](#)]
98. Li, Q.; Hu, Y.; Yang, Q.; Li, X.; Zhang, X.; Yang, H.; Ji, P.; Xi, Y.; Wang, Z.L. A robust constant-voltage DC triboelectric nanogenerator using the ternary dielectric triboelectrification effect. *Adv. Energy Mater.* **2023**, *13*, 2202921. [[CrossRef](#)]
99. Lei, R.; Zhai, H.; Nie, J.; Zhong, W.; Bai, Y.; Liang, X.; Xu, L.; Jiang, T.; Chen, X.; Wang, Z.L. Butterfly-inspired triboelectric nanogenerators with spring-assisted linkage structure for water wave energy harvesting. *Adv. Mater. Technol.* **2019**, *4*, 1800514. [[CrossRef](#)]
100. Zhong, W.; Xu, L.; Yang, X.; Tang, W.; Shao, J.; Chen, B.; Wang, Z.L. Open-book-like triboelectric nanogenerators based on low-frequency roll-swing oscillators for wave energy harvesting. *Nanoscale* **2019**, *11*, 7199–7208. [[CrossRef](#)] [[PubMed](#)]
101. Zhang, C.; Yuan, W.; Zhang, B.; Yang, O.; Liu, Y.; He, L.; Wang, J.; Wang, Z.L. High space efficiency hybrid nanogenerators for effective water wave energy harvesting. *Adv. Funct. Mater.* **2022**, *32*, 2111775. [[CrossRef](#)]
102. Liu, S.; Liang, X.; Chen, P.; Long, H.; Jiang, T.; Wang, Z.L. Multilayered helical spherical triboelectric nanogenerator with charge shuttling for water wave energy harvesting. *Small Methods* **2023**, *7*, 2201392. [[CrossRef](#)]
103. An, J.; Wang, Z.M.; Jiang, T.; Liang, X.; Wang, Z.L. Whirling-folded triboelectric nanogenerator with high average power for water wave energy harvesting. *Adv. Funct. Mater.* **2019**, *29*, 1904867. [[CrossRef](#)]

104. Wang, X.; Gao, Q.; Zhu, M.; Wang, J.; Zhu, J.; Zhao, H.; Wang, Z.L.; Cheng, T. Bioinspired butterfly wings triboelectric nanogenerator with drag amplification for multidirectional underwater-wave energy harvesting. *Appl. Energy* **2022**, *323*, 119648. [[CrossRef](#)]
105. Liang, X.; Jiang, T.; Liu, G.; Xiao, T.; Xu, L.; Li, W.; Xi, F.; Zhang, C.; Wang, Z.L. Triboelectric nanogenerator networks integrated with power management module for water wave energy harvesting. *Adv. Funct. Mater.* **2019**, *29*, 1807241. [[CrossRef](#)]
106. Liang, X.; Jiang, T.; Feng, Y.; Lu, P.; An, J.; Wang, Z.L. Triboelectric nanogenerator network integrated with charge excitation circuit for effective water wave energy harvesting. *Adv. Energy Mater.* **2020**, *10*, 2002123. [[CrossRef](#)]
107. Li, W.; Wan, L.; Lin, Y.; Liu, G.; Qu, H.; Wen, H.; Ding, J.; Ning, H.; Yao, H. Synchronous nanogenerator with intermittent sliding friction self-excitation for water wave energy harvesting. *Nano Energy* **2022**, *95*, 106994. [[CrossRef](#)]
108. Li, G.; Wang, J.; Fu, S.; Shan, C.; Wu, H.; An, S.; Du, Y.; He, W.; Wang, Z.; Liu, W.; et al. A nanogenerator enabled by a perfect combination and synergetic utilization of triboelectrification, charge excitation and electromagnetic induction to reach efficient energy conversion. *Adv. Funct. Mater.* **2023**, *33*, 2213893. [[CrossRef](#)]
109. Li, Y.; Guo, Z.; Zhao, Z.; Gao, Y.; Yang, P.; Qiao, W.; Zhou, L.; Wang, J.; Wang, Z.L. Multi-layered triboelectric nanogenerator incorporated with self-charge excitation for efficient water wave energy harvesting. *Appl. Energy* **2023**, *336*, 120792. [[CrossRef](#)]
110. Han, J.; Liu, Y.; Feng, Y.; Jiang, T.; Wang, Z.L. Achieving a large driving force on triboelectric nanogenerator by wave-driven linkage mechanism for harvesting blue energy toward marine environment monitoring. *Adv. Energy Mater.* **2023**, *13*, 2203219. [[CrossRef](#)]
111. Xu, M.; Zhao, T.; Wang, C.; Zhang, S.L.; Li, Z.; Pan, X.; Wang, Z.L. High power density tower-like triboelectric nanogenerator for harvesting arbitrary directional water wave energy. *ACS Nano* **2019**, *13*, 1932–1939. [[CrossRef](#)]
112. Fu, S.; He, W.; Tang, Q.; Wang, Z.; Liu, W.; Li, Q.; Shan, C.; Long, L.; Hu, C.; Liu, H. An ultrarobust and high-performance rotational hydrodynamic triboelectric nanogenerator enabled by automatic mode switching and charge excitation. *Adv. Mater.* **2022**, *34*, 2105882. [[CrossRef](#)]
113. Wu, H.; Wang, J.; He, W.; Shan, C.; Fu, S.; Li, G.; Zhao, Q.; Liu, W.; Hu, C. Ultrahigh output charge density achieved by charge trapping failure of dielectric polymers. *Energy Environ. Sci.* **2023**, *16*, 2274–2283. [[CrossRef](#)]
114. Li, X.; Xu, L.; Lin, P.; Yang, X.; Wang, H.; Qin, H.; Wang, Z.L. Three-dimensional chiral networks of triboelectric nanogenerators inspired by metamaterial's structure. *Energy Environ. Sci.* **2023**, *16*, 3040–3052. [[CrossRef](#)]
115. Fu, S.; Wu, H.; Shan, C.; Li, K.; He, W.; Li, Q.; Yu, X.; Du, S.; Li, G.; Hu, C. Ultra-durable and high-output triboelectric nanogenerator based on coupling of soft-soft contact and volume effect. *Nano Energy* **2023**, *116*, 108850. [[CrossRef](#)]
116. Zhong, W.; Xu, L.; Wang, H.; Li, D.; Wang, Z.L. Stacked pendulum-structured triboelectric nanogenerators for effectively harvesting low-frequency water wave energy. *Nano Energy* **2019**, *66*, 104108. [[CrossRef](#)]
117. Wang, Y.; Matin Nazar, A.; Wang, J.; Xia, K.; Wang, D.; Ji, X.; Jiao, P. Rolling spherical triboelectric nanogenerators (RS-TENG) under low-frequency ocean wave action. *J. Mar. Sci. Eng.* **2022**, *10*, 5. [[CrossRef](#)]
118. Heo, D.; Son, J.-h.; Kim, D.; Song, M.; Ryu, H.; Kim, S.; Choi, K.; Lin, Z.-H.; Kim, D.; Hong, J.; et al. Charge-accumulating-flutter-based triboelectric nanogenerator via discharge gateway. *Adv. Energy Mater.* **2023**, *13*, 2204239. [[CrossRef](#)]
119. Son, J.-h.; Chung, S.-H.; Cha, K.; Kim, S.; Lin, Z.-H.; Hong, J.; Chung, J.; Lee, S. Ultrahigh performance, serially stackable, breeze driven triboelectric generator via ambient air ionizing channel. *Adv. Mater.* **2023**, *35*, 2300283. [[CrossRef](#)]
120. Zhang, L.; Zhang, B.; Chen, J.; Jin, L.; Deng, W.; Tang, J.; Zhang, H.; Pan, H.; Zhu, M.; Yang, W.; et al. Lawn structured triboelectric nanogenerators for scavenging sweeping wind energy on rooftops. *Adv. Mater.* **2016**, *28*, 1650–1656. [[CrossRef](#)] [[PubMed](#)]
121. Luo, Y.; Chen, P.; Cao, L.N.Y.; Xu, Z.; Wu, Y.; He, G.; Jiang, T.; Wang, Z.L. Durability improvement of breeze-driven triboelectric-electromagnetic hybrid nanogenerator by a travel-controlled approach. *Adv. Funct. Mater.* **2022**, *32*, 2205710. [[CrossRef](#)]
122. Wang, Y.; Huang, T.; Gao, Q.; Li, J.; Wen, J.; Wang, Z.L.; Cheng, T. High-voltage output triboelectric nanogenerator with DC/AC optimal combination method. *Nano Res.* **2022**, *15*, 3239–3245. [[CrossRef](#)]
123. Zhang, B.; Zhang, S.; Li, W.; Gao, Q.; Zhao, D.; Wang, Z.L.; Cheng, T. Self-powered sensing for smart agriculture by electromagnetic-triboelectric hybrid generator. *ACS Nano* **2021**, *15*, 20278–20286. [[CrossRef](#)] [[PubMed](#)]
124. Li, X.; Zhang, C.; Gao, Y.; Zhao, Z.; Hu, Y.; Yang, O.; Liu, L.; Zhou, L.; Wang, J.; Wang, Z.L. A highly efficient constant-voltage triboelectric nanogenerator. *Energy Environ. Sci.* **2022**, *15*, 1334–1345. [[CrossRef](#)]
125. Chen, P.; An, J.; Cheng, R.; Shu, S.; Berbille, A.; Jiang, T.; Wang, Z.L. Rationally segmented triboelectric nanogenerator with a constant direct-current output and low crest factor. *Energy Environ. Sci.* **2021**, *14*, 4523–4532. [[CrossRef](#)]
126. He, W.; Shan, C.; Fu, S.; Wu, H.; Wang, J.; Mu, Q.; Li, G.; Hu, C. Large harvested energy by self-excited liquid suspension triboelectric nanogenerator with optimized charge transportation behavior. *Adv. Mater.* **2023**, *35*, 2209657. [[CrossRef](#)]
127. Liu, D.; Gao, Y.; Zhou, L.; Wang, J.; Wang, Z.L. Recent advances in high-performance triboelectric nanogenerators. *Nano Res.* **2023**, *16*, 11698–11717. [[CrossRef](#)]
128. Yang, H.; Fan, F.R.; Xi, Y.; Wu, W. Design and engineering of high-performance triboelectric nanogenerator for ubiquitous unattended devices. *EcoMat* **2021**, *3*, e12093. [[CrossRef](#)]
129. Liu, L.; Guo, X.; Liu, W.; Lee, C. Recent progress in the energy harvesting technology-from self-powered sensors to self-sustained IoT, and new applications. *Nanomaterials* **2021**, *11*, 2975. [[CrossRef](#)] [[PubMed](#)]
130. Fu, S.; He, W.; Wu, H.; Shan, C.; Du, Y.; Li, G.; Wang, P.; Guo, H.; Chen, J.; Hu, C. High output performance and ultra-durable DC output for triboelectric nanogenerator inspired by primary cell. *Nano-Micro Lett.* **2022**, *14*, 155. [[CrossRef](#)]

131. Ji, P.; Li, Q.; Zhang, X.; Hu, Y.; Han, X.; Zhang, D.; Hu, C.; Xi, Y. Achieving continuous self-powered energy conversion-storage-supply integrated system based on carbon felt. *Adv. Sci.* **2023**, *10*, 2207033. [[CrossRef](#)]
132. Liu, D.; Li, C.; Chen, P.; Zhao, X.; Tang, W.; Wang, Z.L. Sustainable long-term and wide-area environment monitoring network based on distributed self-powered wireless sensing nodes. *Adv. Energy Mater.* **2023**, *13*, 2202691. [[CrossRef](#)]
133. Wu, H.; Wang, J.; Wu, Z.; Kang, S.; Wei, X.; Wang, H.; Luo, H.; Yang, L.; Liao, R.; Wang, Z.L. Multi-parameter optimized triboelectric nanogenerator based self-powered sensor network for broadband aeolian vibration online-monitoring of transmission lines. *Adv. Energy Mater.* **2022**, *12*, 2103654. [[CrossRef](#)]
134. Gui, Y.; Wang, Y.; He, S.; Yang, J. Self-powered smart agriculture real-time sensing device based on hybrid wind energy harvesting triboelectric-electromagnetic nanogenerator. *Energy Convers. Manag.* **2022**, *269*, 116098. [[CrossRef](#)]
135. Li, X.; Luo, J.; Han, K.; Shi, X.; Ren, Z.; Xi, Y.; Ying, Y.; Ping, J.; Wang, Z.L. Stimulation of ambient energy generated electric field on crop plant growth. *Nat. Food* **2022**, *3*, 133–142. [[CrossRef](#)]
136. Liu, L.; Guo, X.; Lee, C. Promoting smart cities into the 5G era with multi-field Internet of Things (IoT) applications powered with advanced mechanical energy harvesters. *Nano Energy* **2021**, *88*, 106304. [[CrossRef](#)]
137. Dai, S.; Li, X.; Jiang, C.; Ping, J.; Ying, Y. Triboelectric nanogenerators for smart agriculture. *InfoMat* **2023**, *5*, e12391. [[CrossRef](#)]
138. Cao, X.; Jie, Y.; Wang, N.; Wang, Z.L. Triboelectric nanogenerators driven self-powered electrochemical processes for energy and environmental science. *Adv. Energy Mater.* **2016**, *6*, 1600665. [[CrossRef](#)]
139. Zhai, N.; Wen, Z.; Chen, X.; Wei, A.; Sha, M.; Fu, J.; Liu, Y.; Zhong, J.; Sun, X. Blue energy collection toward all-hours self-powered chemical energy conversion. *Adv. Energy Mater.* **2020**, *10*, 2001041. [[CrossRef](#)]
140. Han, K.; Luo, J.; Feng, Y.; Xu, L.; Tang, W.; Wang, Z.L. Self-powered electrocatalytic ammonia synthesis directly from air as driven by dual triboelectric nanogenerators. *Energy Environ. Sci.* **2020**, *13*, 2450–2458. [[CrossRef](#)]
141. Zhang, B.; Zhang, C.; Yuan, W.; Yang, O.; Liu, Y.; He, L.; Hu, Y.; Zhou, L.; Wang, J.; Wang, Z.L. Highly stable and eco-friendly marine self-charging power systems composed of conductive polymer supercapacitors with seawater as an electrolyte. *ACS Appl. Mater. Interfaces* **2022**, *14*, 9046–9056. [[CrossRef](#)]
142. Yang, H.; Deng, M.; Zeng, Q.; Zhang, X.; Hu, J.; Tang, Q.; Yang, H.; Hu, C.; Xi, Y.; Wang, Z.L. Polydirectional microvibration energy collection for self-powered multifunctional systems based on hybridized nanogenerators. *ACS Nano* **2020**, *14*, 3328–3336. [[CrossRef](#)]
143. Li, Z.; Chen, J.; Guo, H.; Fan, X.; Wen, Z.; Yeh, M.-H.; Yu, C.; Cao, X.; Wang, Z.L. Triboelectrification-enabled self-powered detection and removal of heavy metal ions in wastewater. *Adv. Mater.* **2016**, *28*, 2983–2991. [[CrossRef](#)] [[PubMed](#)]
144. Li, Z.; Chen, J.; Yang, J.; Su, Y.; Fan, X.; Wu, Y.; Yu, C.; Wang, Z.L. Beta-cyclodextrin enhanced triboelectrification for self-powered phenol detection and electrochemical degradation. *Energy Environ. Sci.* **2015**, *8*, 887–896. [[CrossRef](#)]
145. Gao, S.; Chen, Y.; Su, J.; Wang, M.; Wei, X.; Jiang, T.; Wang, Z.L. Triboelectric nanogenerator powered electrochemical degradation of organic pollutant using Pt-free carbon materials. *ACS Nano* **2017**, *11*, 3965–3972. [[CrossRef](#)] [[PubMed](#)]
146. Yeh, M.-H.; Lin, L.; Yang, P.-K.; Wang, Z.L. Motion-driven electrochromic reactions for self-powered smart window system. *ACS Nano* **2015**, *9*, 4757–4765. [[CrossRef](#)]
147. Zou, Y.; Tan, P.; Shi, B.; Ouyang, H.; Jiang, D.; Liu, Z.; Li, H.; Yu, M.; Wang, C.; Qu, X.; et al. A bionic stretchable nanogenerator for underwater sensing and energy harvesting. *Nat. Commun.* **2019**, *10*, 2695. [[CrossRef](#)] [[PubMed](#)]
148. Wang, X.; Shi, Y.; Yang, P.; Tao, X.; Li, S.; Lei, R.; Liu, Z.; Wang, Z.L.; Chen, X. Fish-wearable data snooping platform for underwater energy harvesting and fish behavior monitoring. *Small* **2022**, *18*, 2107232. [[CrossRef](#)]

Disclaimer/Publisher’s Note: The statements, opinions and data contained in all publications are solely those of the individual author(s) and contributor(s) and not of MDPI and/or the editor(s). MDPI and/or the editor(s) disclaim responsibility for any injury to people or property resulting from any ideas, methods, instructions or products referred to in the content.